

JUSTIFICATION OF A RELAXATION APPROXIMATION FOR THE NAVIER–STOKES–CAHN–HILLIARD SYSTEM

Jan Giesselmann* & Jens Keim† & Fabio Leotta‡ & Christian Rohde§

ABSTRACT

The Navier–Stokes–Cahn–Hilliard (NSCH) system governs the diffuse-interface dynamics of two incompressible and immiscible fluids. We consider a relaxation approximation of the NSCH system that is composed by a system of first-order hyperbolic balance laws and second-order elliptic operators. We prove first that the solutions of an initial boundary value problem for the approximation recover the limiting NSCH system for vanishing relaxation parameters. To cope with the singular limit we exploit the fact that the approximate solutions dissipate an almost quadratic energy, and employ the relative entropy-framework. In the second part of the work we provide numerical evidence for the analytical results, even in flow regimes not covered by the assumptions needed for the theoretical results. Using a novel marker-and-cell conservative finite-difference approach for both the approximation and the limit system, we are able to compute physically relevant interfacial flow problems including Ostwald ripening and high-velocity flow.

Keywords Incompressible two-phase flow · Phase-field modelling · Hyperbolic balance laws · Relative entropy · Marker-and-cell method

MSC classification 76D05 · 35L40 · 65M06

1. Introduction

We consider the viscous motion of two incompressible, immiscible fluids at constant temperature. For the modelling of such two-phase flows there are two major approaches: the sharp-interface approach and the diffuse-interface approach. We consider the diffuse-interface approach such that interfaces are represented as steep but continuous transition zones, with interfacial width controlled by a small parameter $\gamma > 0$. Thereby we focus on the classical Navier–Stokes–Cahn–Hilliard (NSCH) system as it has been proposed in [28] to describe two fluids with matching density, see also [33]. This model is thermodynamically consistent in the sense that it dissipates a free energy functional that is composed of kinetic energy and the Van-der-Waals energy. It has proven to govern flows involving topological changes like the coalescence and breakup of bubbles and droplets. In the last decades the NSCH system has been extended to multiple physical settings; we only mention here extensions to cope with inhomogeneous densities of the two fluids, see, e.g., [2, 5, 16]. For the well-posedness of the resulting initial boundary problems for the NSCH system in the framework of weak and strong solutions we refer to [1, 23, 24]; without any attempt to cover the rich literature.

Despite significant progress (see, e.g., [6, 8, 14, 17]), the numerics for the NSCH system still poses major challenges, most notably in the context of high-velocity regimes. These difficulties are related to the nonlocality induced by the incompressibility constraint and the fourth-order operators in the Cahn–Hilliard evolution. As a remedy in the framework of the incompressible Navier–Stokes equations, approximations based on the artificial compressibility approach have been suggested, see [40]. Notably, this approximation involves a nonlinear first-order hyperbolic transport operator (see [29] for a version with a linear transport operator but nonlinear zeroth-order terms) such that it is accessible for robust numerical methods from the field of hyperbolic balance laws. An artificial compressibility approximation for the NSCH system can be found in the work [25] that relaxes the divergence constraint by an evolution equation for the pressure but keeps the Cahn–Hilliard evolution unchanged. Lower-order hyperbolic approximations or approximations based on the hyperbolic wave operator of the Cahn–Hilliard equations have been suggested in e.g. [13, 18]. The work of [13] relies on a two-stage approximation procedure. First, the Cahn–Hilliard equation is embedded into a system

*Numerical Analysis and Scientific Computing, Department of Mathematics, Technical University of Darmstadt, email: Jan.Giesselmann@tu-darmstadt.de

†Institute of Applied Analysis and Numerical Simulation & Institute of Aerodynamics and Gas Dynamics, University of Stuttgart, email: Jens.Keim@mathematik.uni-stuttgart.de

‡Numerical Analysis and Scientific Computing, Department of Mathematics, Technical University of Darmstadt, email: Fabio.Leotta@tu-darmstadt.de

§Institute of Applied Analysis and Numerical Simulation & Stuttgart Center for Simulation Science, University of Stuttgart, email: Christian.Rohde@mathematik.uni-stuttgart.de

composed of a conservation law for the phase-field variable and a third-order system of evolution equations for the Cahn–Hilliard flux with frictional damping. The Cahn–Hilliard equation is recovered in the high-friction limit. Next, the third-order operators are relaxed using a screened Poisson equation. This results in an approximate system of first-order evolution equations, similar to previously found approximations of the Navier–Stokes–Korteweg models, see [20, 27, 35].

Based on a combination of the artificial compressibility approach for the Navier–Stokes equations, the friction-type approximation, and relaxation of the Cahn–Hilliard equations, a lower-order relaxation approximation of the entire Navier–Stokes–Cahn–Hilliard model has been suggested in [30]. This relaxation approximation comes with three a-priori independent approximation parameters such that the NSCH system is formally recovered if they tend to zero. We note that the relaxation approximation is thermodynamically consistent, i.e., there is a free energy functional that is non-increasing in-time for smooth solutions. For vanishing approximation parameters, the free energy formally collapses to the free energy of the NSCH system. Under reasonable assumptions it has been shown that the involved first-order operator in the lower-order approximate system is hyperbolic. In fact, for this sub-system, the free energy acts as a convex (mathematical) entropy. Due to the hyperbolic structure one can apply also in this case numerical methods from the field of systems of hyperbolic balance laws. First results in one spatial dimension, which have been presented in [30], suggest that it is also possible to address in this way high-velocity flows.

In the present work, we provide a rigorous analytical justification of a slightly modified version of the relaxation approximation introduced in [30] as an approximation of the Navier–Stokes–Cahn–Hilliard system. The modification consists of additional dissipative terms, which can be used to absorb error terms in the relative-entropy inequality, without altering the hyperbolic structure of the first-order operator. All involved systems are shortly reviewed in Section 2. To the best of our knowledge, this is the first result establishing convergence of a fully lower-order relaxation model with hyperbolic first order operator to the NSCH system in the regime of smooth solutions. In addition, our result does not rely on viscosity, i.e., it trivially extends to the Euler–Cahn–Hilliard case.

For the approximate system, we employ a low-regularity entropy solution concept. Our main result, Theorem 3.13 in Section 3, proves that we recover in the limit of vanishing approximation parameters the velocity and phase field solving the initial boundary value problem for the NSCH system, as long as the latter admits a sufficiently regular strong solution. In the proof, we exploit the energetic structure of the relaxation approximation and the NSCH system. We utilize the relative-entropy method (see [12, 15]) and derive quantitative expressions for the error in terms of all three approximation parameters yielding explicit convergence rates in the regime of smooth solutions. A key difficulty, especially in the setting of weak solutions for the relaxation system, arises from the non-convexity of the energy functional of the relaxation system, which prevents a direct application of standard relative-entropy arguments. Another key ingredient of the proof is the construction of an approximate solution to the relaxation system from a given smooth solution of the NSCH system. We use a nontrivial construction, since a straightforward choice would lead to reduced convergence rates, see Remark 3.11 for details.

Section 4 is devoted to the numerical justification of the relaxation approximation by a novel numerical scheme. It is proposed in Section 4.1 as a first-order time-integration scheme for both the NSCH system and the relaxation system such that Chorin’s projection method is recovered in the limit of vanishing approximation parameters. In space, a staggered-mesh conservative finite-difference method is employed. More precisely, we introduce a marker-and-cell (MAC) finite difference scheme for both the target NSCH system and the relaxation approximation. Within this second-order approach, the pressure and the phase field are approximated at the centers of a Cartesian mesh volume whereas the velocity and the Cahn–Hilliard flux are evaluated on the mid points of the boundaries of the cell volumes. We test the full discretization method on one- and two-dimensional settings. The numerical experiments confirm the convergence rates predicted by Theorem 3.13. Moreover, we display results of numerical experiments featuring Ostwald ripening and bubble coalescence scenarios for the relaxation approximation. The latter setup with velocity fields of large magnitude clearly shows that our approach is robust for high-speed flow fields.

Let us note that our approach is different from the MAC finite-difference method for the NSCH system from [32] which relies on the classical work [26] for the incompressible Navier–Stokes equations. The method in [32] builds on the order reduction by the scalar auxiliary variable idea. We follow [39] and discretize the fourth-order operator directly.

We conclude the introduction with some remarks on the use of the relative-entropy method in related frameworks. Closely related to the artificial-compressibility ansatz is the low-Mach number asymptotics, i.e., the passage from the compressible regime to incompressible Navier–Stokes or Euler flow. Rigorous analysis for vanishing Mach number based on relative entropies can be found in [3]. The high-friction limit that connects the damped Navier–Stokes–Korteweg equations to the Cahn–Hilliard equation has been analyzed via relative entropies for convex free energies in, e.g., [11, 20] and for non-convex cases in [10]. With regard to the relaxation of the originally third-order term in the friction-type approximation, we refer to [7]. Finally, we mention the closely related works [4, 22] to approximate third-order operators in dispersive transport.

2. Phase-field modelling for incompressible two-phase flow

We present a short review of the NSCH system and the relaxation approximation together with the respective energy dissipation statements.

2.1. The Navier-Stokes-Cahn-Hilliard system

For $d \in \{2, 3\}$, let $\Omega \subset \mathbb{R}^d$ be an open, bounded set with smooth boundary $\partial\Omega$. This trivially includes the periodic torus case $\Omega = \mathbb{T}^d$ which is used in the analytical Section 3. We denote the outer normal of $\partial\Omega$ by $\mathbf{n} \in \mathcal{S}^{d-1}$.

For time $T > 0$, the classical Navier-Stokes-Cahn-Hilliard (NSCH) system for matched densities from [28] is given by

$$\begin{aligned} \nabla \cdot \mathbf{u} &= 0, \\ \mathbf{u}_t + (\mathbf{u} \cdot \nabla) \mathbf{u} + \nabla p &= -c \nabla \mu(c) + \nu \Delta \mathbf{u}, \quad \text{in } \Omega_T := (0, T) \times \Omega, \\ c_t + \nabla \cdot (c \mathbf{u}) &= \nabla \cdot (\nabla \mu(c)) \end{aligned} \quad (2.1)$$

The hydromechanical unknowns in (2.1) are the pressure (perturbation) $p = p(t, \mathbf{x}) \in \mathbb{R}$ and the velocity field $\mathbf{u} = \mathbf{u}(t, \mathbf{x}) \in \mathbb{R}^d$. For the Cahn-Hilliard part, we have the phase-field variable $c = c(t, \mathbf{x}) \in \mathbb{R}$, which acts as phase indicator.

In (2.1), we denote by $\nu \geq 0$ the constant kinematic viscosity parameter. Thus, inviscid Euler flow is included by choosing $\nu = 0$. The parameter $\gamma > 0$ is the phase-field parameter which is fixed throughout the paper. For the free energy function $W : \mathbb{R} \rightarrow \mathbb{R}$, we make the simple polynomial double-well choice

$$W(c) = \frac{1}{4}(c^2 - 1)^2 \quad (c \in \mathbb{R}). \quad (2.2)$$

Having W defined, the chemical potential in (2.1) is given by $\mu(c) := W'(c) - \gamma \Delta c$.

Note that we consider here a special version of the Cahn-Hilliard equation where densities of both phases are equal and the mobility is supposed to be constant (all set to 1). A generalization of our results to general mobilities and in particular the analysis for the case of different densities, see [2], is much more intricate.

The system (2.1) is complemented with the initial conditions

$$\mathbf{u}(0, \cdot) = \mathbf{u}_0, \quad c(0, \cdot) = c_0 \text{ in } \Omega. \quad (2.3)$$

If $\Omega \neq \emptyset$ holds, a natural choice for boundary conditions is given by

$$\mathbf{u} = \mathbf{0}, \quad \nabla c \cdot \mathbf{n} = 0, \quad \nabla \mu(c) \cdot \mathbf{n} = 0 \text{ on } (0, T) \times \partial\Omega. \quad (2.4)$$

The homogeneous boundary condition $\nabla c \cdot \mathbf{n} = 0$ ensures that the contact angle of a diffuse interface at the boundary $\partial\Omega$ is fixed to be 90° . In Section 3, we are interested in classical solutions for the initial value problem (2.1), (2.3) on $\Omega = \mathbb{T}^d$. By a classical solution we mean a triple $(p, \mathbf{u}, c) : \bar{\Omega}_T \rightarrow \mathbb{R}^{d+2}$ with

$$\begin{aligned} p &\in C^0(\Omega_T), p(\cdot, t) \in C^1(\Omega), \\ \mathbf{u} &\in C^1((0, T); C(\Omega)^d) \cap C^0([0, T]; C^2(\Omega)), \\ c &\in C^1((0, T); C(\Omega)) \cap C([0, T]; C^4(\Omega)), \end{aligned}$$

such that all equations in (2.1), in (2.3), and as the case may be, in (2.4) hold pointwise.

For the wellposedness of solutions for the initial boundary value problem (2.1), (2.3), (2.4) let us refer to [23]. The authors establish a global wellposedness result for a strong solution concept in 2D and for weak solutions in 2D/3D. Our analysis in Section 3 relies on energy techniques. For the NSCH system (2.1), we define the energy expression

$$E[\mathbf{u}, c, \mathbf{d}] = \frac{1}{2}|\mathbf{u}|^2 + W(c) + \frac{\gamma}{2}|\mathbf{d}|^2 \quad (\mathbf{u} \in \mathbb{R}^d, c \in \mathbb{R}, \mathbf{d} \in \mathbb{R}^d), \quad (2.5)$$

which is composed as a sum of the kinetic energy and the classical van der Waals energy if \mathbf{d} is identified with the gradient of the phase field variable. Then we recall the following well-known statement on energy dissipation. Note that all expressions in (2.6) are bounded quantities for a classical solution. The result is formulated for the boundary conditions in (2.4) but holds also for $\Omega = \mathbb{T}^d$.

Theorem 2.1 (Energy dissipation for (2.1)) *Let $(p, \mathbf{u}, c)^T : \bar{\Omega}_T \rightarrow \mathbb{R}^{d+2}$ be a classical solution of the initial boundary value problem for (2.1) satisfying (2.3), (2.4).*

Then, we have for all $t \in [0, T]$ the energy balance relation

$$\int_{\Omega} E[\mathbf{u}, c, \nabla c](t, \mathbf{x}) \, d\mathbf{x} + \int_0^t \int_{\Omega} (|\nabla \mu(c(s, \mathbf{x}))|^2 + \nu |\nabla \mathbf{u}(s, \mathbf{x})|^2) \, d\mathbf{x} ds = \int_{\Omega} E[\mathbf{u}_0, c_0, \nabla c_0](\mathbf{x}) \, d\mathbf{x}. \quad (2.6)$$

2.2. A low-order relaxation approximation of the NSCH system

In [30], an approximation of the NSCH system (2.1) has been suggested that combines the artificial compressibility idea of [40] and the combined friction-type/screened Poisson ansatz as in [13, 35]. These three approximations come with the tuple $\varepsilon = (\alpha, \beta, \delta, \tau) \in (0, 1)^4$ of small approximation parameters. Here we rely on a modification of the model from [30] that we refer to in the sequel as relaxation approximation.

The relaxation approximation of the NSCH system (2.1) writes as

$$\begin{aligned} p_t^\varepsilon + \frac{1}{\alpha} \nabla \cdot \mathbf{u}^\varepsilon &= 0, \\ \mathbf{u}_t^\varepsilon + (\mathbf{u}^\varepsilon \cdot \nabla) \mathbf{u}^\varepsilon + \frac{1}{2} (\nabla \cdot \mathbf{u}^\varepsilon) \mathbf{u}^\varepsilon + \nabla p^\varepsilon &= -c^\varepsilon \nabla \left(W'(c^\varepsilon) + \frac{1}{\beta} (c^\varepsilon - \omega^\varepsilon) \right) \\ &\quad + \nu \Delta \mathbf{u}^\varepsilon + (\lambda + \nu) \nabla (\nabla \cdot \mathbf{u}^\varepsilon), \\ c_t^\varepsilon + \nabla \cdot (c^\varepsilon \mathbf{u}^\varepsilon) + \nabla \cdot \mathbf{v}^\varepsilon &= \tau \Delta c^\varepsilon, \quad \text{in } \Omega_T. \\ \mathbf{v}_t^\varepsilon + \frac{1}{\delta} \nabla \left(W'(c^\varepsilon) + \frac{1}{\beta} c^\varepsilon \right) &= -\frac{\mathbf{v}^\varepsilon}{\delta} + \frac{1}{\delta \beta} \nabla \omega^\varepsilon + \nabla (\nabla \cdot \mathbf{v}^\varepsilon), \\ -\gamma \Delta \omega^\varepsilon + \frac{1}{\beta} \omega^\varepsilon &= \frac{1}{\beta} c^\varepsilon \end{aligned} \quad (2.7)$$

The unknowns are the pressure $p^\varepsilon = p^\varepsilon(t, \mathbf{x})$, the velocity $\mathbf{u}^\varepsilon = \mathbf{u}^\varepsilon(t, \mathbf{x})$, the phase-field variable $c^\varepsilon = c^\varepsilon(t, \mathbf{x})$, the Cahn-Hilliard flux $\mathbf{v}^\varepsilon = \mathbf{v}^\varepsilon(t, \mathbf{x})$, and the relaxation variable $\omega^\varepsilon = \omega^\varepsilon(t, \mathbf{x})$.

The modifications in the relaxation approximation (2.7) refer to three items: 1) we consider for the viscous part of the stress tensor the kinematic shear viscosity and the (artificial) bulk viscosity $\lambda > 0$. The latter has not been accounted for in [30]; 2) we add the term $\tau \Delta c^\varepsilon$ in the conservation law for the phase field variable c^ε ; 3) we add the regularization term $\nabla (\nabla \cdot \mathbf{v}^\varepsilon)$ in the equations for the Cahn-Hilliard flux.

These three extensions are needed to provide additional dissipation terms in the proof of Theorem 3.13 below. We will see that the terms $(\lambda + \nu) \nabla (\nabla \cdot \mathbf{u}^\varepsilon)$, $\tau \Delta c^\varepsilon$ and $\nabla (\nabla \cdot \mathbf{v}^\varepsilon)$ vanish in the limit when $|\varepsilon| \rightarrow 0$.

The system (2.7) is endowed with the initial conditions

$$p^\varepsilon(0, \cdot) = p_0^\varepsilon, \quad \mathbf{u}^\varepsilon(0, \cdot) = \mathbf{u}_0^\varepsilon, \quad \mathbf{v}^\varepsilon(0, \cdot) = \mathbf{v}_0^\varepsilon, \quad c^\varepsilon(0, \cdot) = c_0^\varepsilon \text{ in } \Omega, \quad (2.8)$$

and, if applicable, the boundary conditions

$$\mathbf{u}^\varepsilon = \mathbf{0}, \quad \nabla \omega^\varepsilon \cdot \mathbf{n} = 0, \quad \nabla c^\varepsilon \cdot \mathbf{n} = 0, \quad \mathbf{v}^\varepsilon \cdot \mathbf{n} = 0 \text{ on } (0, T) \times \partial\Omega. \quad (2.9)$$

Note that the Neumann condition for the phase field and the Neumann condition for the chemical potential μ in (2.4) are transferred to a Neumann condition for ω^ε and a no-flux condition for the Cahn-Hilliard flux, respectively. Analogously as for the NSCH system, a classical solution of the relaxation approximation (2.7) that satisfies (2.8) is a tuple of functions $\mathbf{U}^\varepsilon = (p^\varepsilon, \mathbf{u}^\varepsilon, c, \mathbf{v}^\varepsilon, \omega^\varepsilon)$ such that

$$\begin{aligned} p^\varepsilon &\in C^1((0, T) \times \Omega) \cap C([0, T] \times \overline{\Omega}), \\ \mathbf{u}^\varepsilon &\in C^1((0, T); C(\Omega; \mathbb{R}^d)) \cap C([0, T]; C^2(\overline{\Omega}; \mathbb{R}^d)), \\ c^\varepsilon &\in C^1((0, T); C(\Omega)) \cap C([0, T]; C^1(\overline{\Omega})), \\ \mathbf{v}^\varepsilon &\in C^1((0, T); C(\Omega; \mathbb{R}^d)) \cap C([0, T]; C^2(\overline{\Omega})), \\ \omega^\varepsilon &\in C^1((0, T) \times \Omega) \cap C([0, T]; C^2(\overline{\Omega})) \end{aligned}$$

holds, and such that the equations in (2.7) and (2.8) are satisfied. We are not aware of any global well-posedness results for classical solutions but note that the initial value problem on \mathbb{R}^d can be analyzed following the results on hyperbolic-parabolic systems in [38]. For our analysis, we will work with a weaker solution concept that is provided in Definition 3.2 and relies on the energy structure of the relaxation approximation. Indeed, for the energy term

$$E^\varepsilon[p, \mathbf{u}, c, \mathbf{v}, \omega, \mathbf{e}] = \frac{\alpha}{2} p^2 + \frac{1}{2} |\mathbf{u}|^2 + \frac{\delta}{2} |\mathbf{v}|^2 + W(c) + \frac{1}{2\beta} (c - \omega)^2 + \frac{\gamma}{2} |\mathbf{e}|^2 \quad ((p, \mathbf{u}, c, \mathbf{v}, \omega, \mathbf{e}) \in \mathbb{R}^{3d+3}), \quad (2.10)$$

we obtain as in [30] the statement

Theorem 2.2 (Energy dissipation for (2.7)) For $\varepsilon \in (0, 1)^4$, let $(p^\varepsilon, \mathbf{u}^\varepsilon, c^\varepsilon, \mathbf{v}^\varepsilon, \omega^\varepsilon)^T : \bar{\Omega}_T \rightarrow \mathbb{R}^{2d+3}$ be a classical solution of (2.7), (2.8) and (2.9): Then we have for all $t \in [0, T]$ the energy balance equation

$$\begin{aligned} & \int_{\Omega} E^\varepsilon [p^\varepsilon, \mathbf{u}^\varepsilon, c^\varepsilon, \mathbf{v}^\varepsilon, \omega^\varepsilon] \, d\mathbf{x} \\ &= \int_{\Omega} E^\varepsilon [p_0^\varepsilon, \mathbf{u}_0^\varepsilon, c_0^\varepsilon, \mathbf{v}_0^\varepsilon, \omega^\varepsilon(0, \cdot), \nabla \omega^\varepsilon(0, \cdot)] \, d\mathbf{x} \\ & \quad - \int_0^t \int_{\Omega} \nu |\nabla \mathbf{u}^\varepsilon|^2 + (\lambda + \nu)(\nabla \cdot \mathbf{u}^\varepsilon)^2 + \tau |\nabla c^\varepsilon|^2 + |\mathbf{v}^\varepsilon|^2 + \delta (\nabla \cdot \mathbf{v}^\varepsilon)^2 \, d\mathbf{x} ds. \end{aligned}$$

One readily sees that the energy dissipation rate statement formally reduces to (2.6) if the approximation parameters vanish. Note that the energy (2.10) is non-convex due to the presence of the double-well function W .

3. Convergence of the relaxation approximation

Throughout this section, we will consider the case of periodic boundary conditions, i.e., $\Omega = \mathbb{T}^d$ the torus. Note however, that a generalization of the presented results to the case of physical boundary conditions is possible; cf. Remark 3.15. Our main goal is to show that solutions of (2.7) converge to (2.1) in the $|\varepsilon| \rightarrow 0$ limit, as long as (2.1) admits a classical solution with additional regularity; cf. Theorem 3.13. A crucial step in this endeavor is to study the stability of solutions to (2.7), i.e., their closeness to solutions of

$$\begin{cases} p_t^\varepsilon + \frac{1}{\alpha} \nabla \cdot \mathbf{u}^\varepsilon &= -\mathcal{R}_1, \\ \mathbf{u}_t^\varepsilon + (\mathbf{u}^\varepsilon \cdot \nabla) \mathbf{u}^\varepsilon + \frac{1}{2} (\nabla \cdot \mathbf{u}^\varepsilon) \mathbf{u}^\varepsilon + \nabla p^\varepsilon &= -c^\varepsilon \nabla \left(W'(c^\varepsilon) + \frac{1}{\beta} (c^\varepsilon - \omega^\varepsilon) \right) \\ & \quad + \nu \Delta \mathbf{u}^\varepsilon + (\lambda + \nu) \nabla (\nabla \cdot \mathbf{u}^\varepsilon) - \mathcal{R}_2, \\ c_t^\varepsilon + \nabla \cdot (c^\varepsilon \mathbf{u}^\varepsilon) + \nabla \cdot \mathbf{v}^\varepsilon &= \tau \Delta c^\varepsilon - \mathcal{R}_3, \\ \mathbf{v}_t^\varepsilon + \frac{1}{\delta} \nabla \left(W'(c^\varepsilon) + \frac{1}{\beta} c^\varepsilon \right) &= -\frac{\mathbf{v}^\varepsilon}{\delta} + \frac{1}{\delta \beta} \nabla \omega^\varepsilon + \nabla (\nabla \cdot \mathbf{v}^\varepsilon) - \mathcal{R}_4, \\ -\gamma \Delta \omega^\varepsilon + \frac{1}{\beta} \omega^\varepsilon &= \frac{1}{\beta} c^\varepsilon - \mathcal{R}_5 \end{cases}, \quad (3.1)$$

w.r.t. given residuals $\mathcal{R}_i \in C([0, T] \times \Omega)$, $i \in \{1, 2, 3, 4, 5\}$, and initial data.

In the following, solutions to the relaxation system (2.7) will be denoted as $\mathbf{U} = [p, \mathbf{u}, c, \mathbf{v}, \omega]$ while solutions to the relaxation system with residuals (3.1) will be denoted as $\bar{\mathbf{U}} = [\bar{p}, \bar{\mathbf{u}}, \bar{c}, \bar{\mathbf{v}}, \bar{\omega}]$, i.e., in both cases we drop the ε to increase readability.

We will study the stability of (2.7) via a relative energy analysis for the energy given in (2.10). In this analysis, we will compare higher-regularity solutions to the NSCH system (2.1) – interpreted appropriately as classical solutions to the relaxation system with residuals (3.1), details will be provided in Proposition 3.12 – with weak solutions to the relaxation system (2.7). We thus formulate the following solution concepts.

Definition 3.1 (Classical solutions to the relaxation system with residuals) A classical solution to (3.1) is a tuple of functions $\bar{\mathbf{U}} = [\bar{p}, \bar{\mathbf{u}}, \bar{c}, \bar{\mathbf{v}}, \bar{\omega}]$ such that

$$\begin{aligned} \bar{p} &\in C^1((0, T) \times \Omega) \cap C([0, T] \times \Omega) \\ \bar{\mathbf{u}} &\in C^1((0, T); C(\Omega; \mathbb{R}^d)) \cap C([0, T]; C^2(\Omega; \mathbb{R}^d)) \\ \bar{c} &\in C^1((0, T); C(\Omega)) \cap C([0, T]; C^1(\Omega)) \\ \bar{\mathbf{v}} &\in C^1((0, T); C(\Omega; \mathbb{R}^d)) \cap C([0, T]; C^2(\Omega)) \\ \bar{\omega} &\in C^1((0, T) \times \Omega) \cap C([0, T]; C^2(\Omega)), \end{aligned}$$

and the equations in (3.1) and initial conditions hold in a pointwise sense.

Definition 3.2 (Weak solutions to the relaxation system) A weak solution to (2.7) is a tuple of functions $\mathbf{U} = [p, \mathbf{u}, c, \mathbf{v}, \omega]$ with

$$\begin{aligned} p &\in H^1(0, T; L^2(\Omega)) \cap L^\infty(0, T; L^2(\Omega)) \\ \mathbf{u} &\in L^2(0, T; H^1(\Omega; \mathbb{R}^d)) \cap L^\infty(0, T; L^2(\Omega; \mathbb{R}^d)) \\ c &\in L^2(0, T; H^1(\Omega)) \cap L^\infty(0, T; L^4(\Omega)) \\ \mathbf{v} &\in L^2(0, T; H_{\text{div}}(\Omega; \mathbb{R}^d)) \cap L^\infty(0, T; L^2(\Omega)) \\ \omega &\in H^1((0, T) \times \Omega), \end{aligned}$$

where $H_{\text{div}}(\Omega; \mathbb{R}^d) = \{\mathbf{v} \in L^2(\Omega; \mathbb{R}^d) \mid \nabla \cdot \mathbf{v} \in L^2(\Omega; \mathbb{R}^d)\}$ and such that for any $0 \leq t_1 < t_2 \leq T$ there holds

$$\begin{aligned} p_t + \frac{1}{\alpha} \nabla \cdot \mathbf{u} &= 0, \\ \int_{t_1}^{t_2} \int_{\Omega} \mathbf{u} \cdot \varphi_t - (\mathbf{u} \cdot \nabla) \mathbf{u} \cdot \varphi - \frac{1}{2} (\nabla \cdot \mathbf{u}) \mathbf{u} \cdot \varphi + p \nabla \cdot \varphi \, d\mathbf{x} dt &= \int_{t_1}^{t_2} \int_{\Omega} c \nabla \left(W'(c) + \frac{1}{\beta} (c - \omega) \right) \cdot \varphi \\ &\quad + \nu \nabla \mathbf{u} : \nabla \varphi + (\lambda + \nu) \nabla \cdot \mathbf{u} \nabla \cdot \varphi \, d\mathbf{x} dt \\ &\quad + \left[\int_{\Omega} \mathbf{u} \cdot \varphi \, d\mathbf{x} \right]_{t_1}^{t_2}, \\ \int_{t_1}^{t_2} \int_{\Omega} c \varphi_t - \varphi \nabla \cdot (c \mathbf{u}) - \varphi \nabla \cdot \mathbf{v} \, d\mathbf{x} dt &= \int_{t_1}^{t_2} \int_{\Omega} \tau \nabla c \cdot \nabla \varphi \, d\mathbf{x} dt + \left[\int_{\Omega} c \varphi \, d\mathbf{x} \right]_{t_1}^{t_2}, \quad (3.2) \\ \int_{t_1}^{t_2} \int_{\Omega} \mathbf{v} \cdot \psi_t + \frac{1}{\delta} \left(W'(c) + \frac{1}{\beta} (c - \omega) \right) \nabla \cdot \psi \, d\mathbf{x} dt &= \int_{t_1}^{t_2} \int_{\Omega} \frac{1}{\delta} \mathbf{v} \cdot \psi + \nabla \cdot \mathbf{v} \nabla \cdot \psi \, d\mathbf{x} dt \\ &\quad + \left[\int_{\Omega} \mathbf{v} \cdot \psi \, d\mathbf{x} \right]_{t_1}^{t_2}, \\ \int_{\Omega} \gamma \nabla \omega \cdot \nabla \xi \, d\mathbf{x} &= \int_{\Omega} \frac{1}{\beta} (c - \omega) \xi \, d\mathbf{x} \end{aligned}$$

for arbitrary test functions $\varphi, \psi \in C^\infty([0, T] \times \Omega; \mathbb{R}^d)$, $\varphi \in C^\infty([0, T] \times \Omega)$, $\xi \in C^\infty(\Omega)$.

The initial conditions are imposed strongly for the pressure and weakly for the other terms, i.e.,

$$p(0, \cdot) = p_0, \quad \lim_{t \rightarrow 0^+} \int_{\Omega} (\mathbf{u}, c, \mathbf{v}) \cdot \Phi \, d\mathbf{x} = \int_{\Omega} (\mathbf{u}_0, c_0, \mathbf{v}_0) \cdot \Phi \, d\mathbf{x}, \quad (3.3)$$

for all $\Phi \in C^\infty(\Omega; \mathbb{R}^d) \times C^\infty(\Omega) \times C^\infty(\Omega; \mathbb{R}^d)$.

Furthermore, for all $\psi \in C_c^\infty([0, T] \times \Omega)$, $\psi \geq 0$, we demand that the energy inequality

$$\int_0^T \int_{\Omega} E \psi_t + \mathbf{Q} \cdot \nabla \psi \, d\mathbf{x} dt \geq \int_0^T \int_{\Omega} S \psi \, d\mathbf{x} dt - \int_{\Omega} [E \psi](0, \cdot) \, d\mathbf{x}, \quad (3.4)$$

holds with

$$E := E^\varepsilon(\mathbf{U}), \quad (3.5)$$

$$\begin{aligned} \mathbf{Q} = \mathbf{Q}[\mathbf{U}] &:= p \mathbf{u} + \frac{1}{2} |\mathbf{u}|^2 \mathbf{u} + \left(W(c) + \frac{1}{\beta} (c - \omega) \right) (\mathbf{c} \mathbf{u} + \mathbf{v}) \\ &\quad - (\nu \nabla \mathbf{u} + (\lambda + \nu) (\nabla \cdot \mathbf{u})) \mathbf{u} - \tau c \nabla c - (\nabla \cdot \mathbf{v}) \mathbf{v} - \gamma \omega_t \nabla \omega, \end{aligned} \quad (3.6)$$

$$S = S[\mathbf{U}] := \lambda |\nabla \mathbf{u}|^2 + (\lambda + \nu) (\nabla \cdot \mathbf{u})^2 + \tau |\nabla c|^2 + \frac{1}{\delta} |\mathbf{v}|^2 + (\nabla \cdot \mathbf{v})^2. \quad (3.7)$$

3.1. The relative energy analysis

Note that in the following, we write $a \lesssim b$ if there exists a constant $k \geq 0$ that is independent of $\varepsilon, \nu, \lambda, \gamma$ such that $a \leq kb$.

The (full) relative energy between two states $\mathbf{U} = (p, \mathbf{u}, c, \mathbf{v}, \omega, \mathbf{e})$, $\bar{\mathbf{U}} = (\bar{p}, \bar{\mathbf{u}}, \bar{c}, \bar{\mathbf{v}}, \bar{\omega}, \bar{\mathbf{e}}) \in \mathbb{R}^{3d+3}$ is given by

$$\begin{aligned}\tilde{\eta}^\varepsilon(\mathbf{U}, \bar{\mathbf{U}}) := & \frac{\alpha}{2}(p - \bar{p})^2 + W(c) - W(\bar{c}) - W'(\bar{c})(c - \bar{c}) + \frac{1}{2\beta}(c - \omega - (\bar{c} - \bar{\omega}))^2 \\ & + \frac{1}{2}|\mathbf{u} - \bar{\mathbf{u}}|^2 + \frac{\delta}{2}|\mathbf{v} - \bar{\mathbf{v}}|^2 + \frac{\gamma}{2}|\mathbf{e} - \bar{\mathbf{e}}|^2.\end{aligned}\quad (3.8)$$

Due to the double-well structure of W , the relative energy $\tilde{\eta}^\varepsilon$ is not necessarily nonnegative. This is unfavorable for a subsequent Gronwall argument. However, by disregarding the non-convex part of W and adding $\frac{1}{2}(c - \bar{c})^2$, we can define the *reduced relative energy*

$$\begin{aligned}\eta^\varepsilon(\mathbf{U}, \bar{\mathbf{U}}) := & \frac{\alpha}{2}(p - \bar{p})^2 + \frac{1}{4}c^4 - \frac{1}{4}\bar{c}^4 - \bar{c}^3(c - \bar{c}) + \frac{1}{2\beta}(c - \omega - (\bar{c} - \bar{\omega}))^2 \\ & + \frac{1}{2}|\mathbf{u} - \bar{\mathbf{u}}|^2 + \frac{\delta}{2}|\mathbf{v} - \bar{\mathbf{v}}|^2 + \frac{\gamma}{2}|\mathbf{e} - \bar{\mathbf{e}}|^2 + \frac{1}{2}(c - \bar{c})^2,\end{aligned}\quad (3.9)$$

which is nonnegative. Also, note that the reduced relative energy allows us to bound

$$(c - \bar{c})^4 \lesssim \eta^\varepsilon,$$

due to the following proposition.

Proposition 3.3 *There holds*

$$0 \leq (2 - \sqrt{3})(c - \bar{c})^4 \leq c^4 - \bar{c}^4 - 4\bar{c}^3(c - \bar{c}), \quad (3.10)$$

for all $c, \bar{c} \in \mathbb{R}$.

Proof: First note that

$$c^4 - \bar{c}^4 = (c^3 + c^2\bar{c} + \bar{c}^2c + \bar{c}^3)(c - \bar{c}), \quad (3.11)$$

thus

$$\begin{aligned}c^4 - \bar{c}^4 - 4\bar{c}^3(c - \bar{c}) &= (c^3 + c^2\bar{c} + \bar{c}^2c - 3\bar{c}^3)(c - \bar{c}) \\ &= (c^2 + 2c\bar{c} + 3\bar{c}^2)(c - \bar{c})^2,\end{aligned}\quad (3.12)$$

while

$$c^2 + 2c\bar{c} + 3\bar{c}^2 = (c - \bar{c}) \begin{pmatrix} 1 & 1 \\ 1 & 3 \end{pmatrix} \begin{pmatrix} c \\ \bar{c} \end{pmatrix}. \quad (3.13)$$

Finally, the matrix $\begin{pmatrix} 1 & 1 \\ 1 & 3 \end{pmatrix}$ is diagonalizable with eigenvalues $\lambda_\pm = 2 \pm \sqrt{3}$ and thus the claim follows. \square

Furthermore, since

$$\eta^\varepsilon = \tilde{\eta}^\varepsilon + (c - \bar{c})^2, \quad (3.14)$$

a Gronwall argument for the reduced relative energy η^ε becomes available, once we appropriately bound the time evolution of the full relative energy $\tilde{\eta}^\varepsilon$ and of $(c - \bar{c})^2$. We start with the former.

Lemma 3.4 (Growth rate of the full relative energy) *Let \mathbf{U} be a weak solution to (2.7) and let $\bar{\mathbf{U}}$ be a classical solution to (3.1). Then, for every $t \leq T$ there holds the following.*

$$\begin{aligned}
 \int_{\Omega} \tilde{\eta}^{\varepsilon}(\mathbf{U}, \bar{\mathbf{U}})(t, \mathbf{x}) d\mathbf{x} &\leq \int_{\Omega} \tilde{\eta}^{\varepsilon}(\mathbf{U}, \bar{\mathbf{U}})(0, \mathbf{x}) d\mathbf{x} + \int_0^t \int_{\Omega} -6\tau(c - \bar{c})\nabla(c - \bar{c}) \cdot \nabla \bar{c} - 3\tau(c - \bar{c})^2 \nabla(c - \bar{c}) \cdot \nabla \bar{c} \\
 &\quad + \tau|\nabla(c - \bar{c})|^2 - (W'(c) - W'(\bar{c}) - W''(\bar{c})(c - \bar{c}))\nabla \cdot (\bar{c}\bar{\mathbf{u}} + \bar{\mathbf{v}}) - \delta(\nabla \cdot (\mathbf{v} - \bar{\mathbf{v}}))^2 \\
 &\quad - \left(\frac{1}{2}(c - \bar{c})^2 W''(\bar{c}) + \frac{1}{3}(c - \bar{c})^3 W'''(\bar{c}) + \frac{3}{4}(c - \bar{c})^4 \right) \nabla \cdot \bar{\mathbf{u}} - |\mathbf{v} - \bar{\mathbf{v}}|^2 \\
 &\quad + \left(\frac{1}{2}(c - \bar{c})^2 W'''(\bar{c}) + (c - \bar{c})^3 \right) \bar{\mathbf{u}} \cdot \nabla \bar{c} - (c - \bar{c})(\mathbf{u} - \bar{\mathbf{u}}) \cdot \nabla W'(\bar{c}) \\
 &\quad - (c - \bar{c})(\mathbf{u} - \bar{\mathbf{u}}) \cdot \nabla(\bar{c} - \bar{\omega}) - \frac{1}{2\beta}(c - \omega - (\bar{c} - \bar{\omega}))^2 \nabla \cdot \bar{\mathbf{u}} - \frac{\tau}{2\beta}|\nabla(c - \bar{c})|^2 \\
 &\quad + \gamma \frac{|\nabla(\omega - \bar{\omega})|^2}{2} \nabla \cdot \bar{\mathbf{u}} + \gamma (\nabla(\omega - \bar{\omega}) \otimes \nabla(\omega - \bar{\omega})) : \nabla \bar{\mathbf{u}} + \frac{\tau}{2\beta}|\nabla(\omega - \bar{\omega})|^2 \\
 &\quad + \gamma(\omega - \bar{\omega}) \nabla(\omega - \bar{\omega}) \cdot \nabla(\nabla \cdot \bar{\mathbf{u}}) - \nabla \bar{\mathbf{u}} : ((\mathbf{u} - \bar{\mathbf{u}}) \otimes (\mathbf{u} - \bar{\mathbf{u}})) \\
 &\quad - \frac{1}{2}(\nabla \cdot (\mathbf{u} - \bar{\mathbf{u}})) \bar{\mathbf{u}} \cdot (\mathbf{u} - \bar{\mathbf{u}}) - \nu|\nabla(\mathbf{u} - \bar{\mathbf{u}})|^2 - (\lambda + \nu)(\nabla \cdot (\mathbf{u} - \bar{\mathbf{u}}))^2 \\
 &\quad + \alpha \mathcal{R}_1(p - \bar{p}) + \mathcal{R}_2(\mathbf{u} - \bar{\mathbf{u}}) + \frac{1}{\beta} \mathcal{R}_3(c - \omega - (\bar{c} - \bar{\omega})) + \delta \mathcal{R}_4(\mathbf{v} - \bar{\mathbf{v}}) \\
 &\quad + \mathcal{R}_5(\omega_t - \bar{\omega}_t) + \mathcal{R}_3 W''(\bar{c})(c - \bar{c}) - (\omega - \bar{\omega}) \bar{\mathbf{u}} \cdot \nabla \mathcal{R}_5 d\mathbf{x} ds. \tag{3.15}
 \end{aligned}$$

Proof: For ease of presentation, we will undertake all computations in this proof for a classical solution \mathbf{U} . The generalization to weak solutions \mathbf{U} is straightforward; cf. e.g. the weak-strong uniqueness proof in [12].

We first compute the time evolution of $\tilde{\eta}^{\varepsilon}(\mathbf{U}, \bar{\mathbf{U}}) \hat{=} \tilde{\eta}^{\varepsilon}$ rather naively and then regroup appropriately. According to the evolution equations and after noticing some simple cancellations, the growth rate of the relative energy takes the preliminary form

$$\begin{aligned}
 \partial_t \tilde{\eta}^{\varepsilon} &= -(p - \bar{p}) \nabla \cdot (\mathbf{u} - \bar{\mathbf{u}}) + \alpha \mathcal{R}_1(p - \bar{p}) \\
 &\quad - (W'(c) - W'(\bar{c})) \nabla \cdot (c\mathbf{u}) + W''(\bar{c})(c - \bar{c}) \nabla \cdot (\bar{c}\bar{\mathbf{u}}) \\
 &\quad - (W'(c) - W'(\bar{c})) \nabla \cdot \mathbf{v} + W''(\bar{c})(c - \bar{c}) \nabla \cdot \bar{\mathbf{v}} + \mathcal{R}_3 W''(\bar{c})(c - \bar{c}) \\
 &\quad + \tau(W'(c) - W'(\bar{c})) \Delta c - \tau W''(\bar{c})(c - \bar{c}) \Delta \bar{c} + \frac{\tau}{\beta}(c - \omega - (\bar{c} - \bar{\omega})) \Delta(c - \bar{c}) \\
 &\quad - \frac{1}{\beta}(c - \omega - (\bar{c} - \bar{\omega})) \nabla \cdot (c\mathbf{u} - \bar{c}\bar{\mathbf{u}}) - \frac{1}{\beta}(c - \omega - (\bar{c} - \bar{\omega})) \nabla \cdot (\mathbf{v} - \bar{\mathbf{v}}) + \frac{1}{\beta} \mathcal{R}_3(c - \omega - (\bar{c} - \bar{\omega})) \\
 &\quad - ((\mathbf{u} \cdot \nabla)\mathbf{u} - (\bar{\mathbf{u}} \cdot \nabla)\bar{\mathbf{u}}) \cdot (\mathbf{u} - \bar{\mathbf{u}}) - \frac{1}{2}((\nabla \cdot \mathbf{u})\mathbf{u} - (\nabla \cdot \bar{\mathbf{u}})\bar{\mathbf{u}}) \cdot (\mathbf{u} - \bar{\mathbf{u}}) \\
 &\quad - (\mathbf{u} - \bar{\mathbf{u}}) \cdot \nabla(p - \bar{p}) - (c \nabla W'(c) - \bar{c} \nabla W'(\bar{c})) \cdot (\mathbf{u} - \bar{\mathbf{u}}) \\
 &\quad - \frac{1}{\beta}(c \nabla(c - \omega) - \bar{c} \nabla(\bar{c} - \bar{\omega})) \cdot (\mathbf{u} - \bar{\mathbf{u}}) + \nu \Delta(\mathbf{u} - \bar{\mathbf{u}}) \cdot (\mathbf{u} - \bar{\mathbf{u}}) + \mathcal{R}_2(\mathbf{u} - \bar{\mathbf{u}}) \\
 &\quad - \nabla(W'(c) - W'(\bar{c})) \cdot (\mathbf{v} - \bar{\mathbf{v}}) - |\mathbf{v} - \bar{\mathbf{v}}|^2 - \frac{1}{\beta}(\mathbf{v} - \bar{\mathbf{v}}) \cdot \nabla(c - \omega - (\bar{c} - \bar{\omega})) \\
 &\quad + \delta \Delta(\mathbf{v} - \bar{\mathbf{v}}) \cdot (\mathbf{v} - \bar{\mathbf{v}}) + \delta \mathcal{R}_4(\mathbf{v} - \bar{\mathbf{v}}) + \mathcal{R}_5(\omega_t - \bar{\omega}_t). \tag{3.16}
 \end{aligned}$$

Let us group some related terms and study them separately, i.e.,

$$I_1 := -(W'(c) - W'(\bar{c})) \nabla \cdot \mathbf{v} + W''(\bar{c})(c - \bar{c}) \nabla \cdot \bar{\mathbf{v}} - \nabla(W'(c) - W'(\bar{c})) \cdot (\mathbf{v} - \bar{\mathbf{v}}), \tag{3.17}$$

$$I_2 := -(W'(c) - W'(\bar{c})) \nabla \cdot (c\mathbf{u}) + W''(\bar{c})(c - \bar{c}) \nabla \cdot (\bar{c}\bar{\mathbf{u}}) - (c \nabla W'(c) - \bar{c} \nabla W'(\bar{c})) \cdot (\mathbf{u} - \bar{\mathbf{u}}), \tag{3.18}$$

$$I_3 := \tau(W'(c) - W'(\bar{c})) \Delta c - \tau W''(\bar{c})(c - \bar{c}) \Delta \bar{c}, \tag{3.19}$$

$$I_4 := -\frac{1}{\beta}(c \nabla(c - \omega) - \bar{c} \nabla(\bar{c} - \bar{\omega})) \cdot (\mathbf{u} - \bar{\mathbf{u}}) - \frac{1}{\beta}(c - \omega - (\bar{c} - \bar{\omega})) \nabla \cdot (c\mathbf{u} - \bar{c}\bar{\mathbf{u}}). \tag{3.20}$$

Now,

$$I_1 = -\nabla \cdot [(W'(c) - W'(\bar{c}))(\mathbf{v} - \bar{\mathbf{v}})] - (W'(c) - W'(\bar{c}) - W''(\bar{c})(c - \bar{c})) \nabla \cdot \bar{\mathbf{v}}, \tag{3.21}$$

and, similarly,

$$\begin{aligned} I_2 = & -\nabla \cdot [(W'(c) - W'(\bar{c}))(c\mathbf{u} - \bar{c}\bar{\mathbf{u}})] - (W'(c) - W'(\bar{c}) - W''(\bar{c})(c - \bar{c}))\nabla \cdot (\bar{c}\bar{\mathbf{u}}) \\ & + (c - \bar{c})\bar{\mathbf{u}} \cdot \nabla(W'(c) - W'(\bar{c})) - (c - \bar{c})(\mathbf{u} - \bar{\mathbf{u}}) \cdot \nabla W'(\bar{c}), \end{aligned} \quad (3.22)$$

where, by Taylor expansion,

$$\begin{aligned} (c - \bar{c})\nabla(W'(c) - W'(\bar{c})) &= (c - \bar{c})\nabla \left(W''(\bar{c})(c - \bar{c}) + \frac{W'''(\bar{c})}{2}(c - \bar{c})^2 + (c - \bar{c})^3 \right) \\ &= \nabla \left[\frac{1}{2}(c - \bar{c})^2 W''(\bar{c}) + \frac{1}{3}(c - \bar{c})^3 W'''(\bar{c}) + (c - \bar{c})^4 \right] \\ &\quad + \frac{1}{2}(c - \bar{c})^2 \nabla W''(\bar{c}) + \frac{1}{6}(c - \bar{c})^3 \nabla W'''(\bar{c}), \end{aligned} \quad (3.23)$$

since W is a fourth-order polynomial. Thus, we can rearrange I_2 as

$$\begin{aligned} I_2 = & -\nabla \cdot [(W'(c) - W'(\bar{c}))(c\mathbf{u} - \bar{c}\bar{\mathbf{u}})] \\ & + \nabla \cdot \left[\left(\frac{1}{2}(c - \bar{c})^2 W''(\bar{c}) + \frac{1}{3}(c - \bar{c})^3 W'''(\bar{c}) + \frac{1}{4}(c - \bar{c})^4 \right) \bar{\mathbf{u}} \right] \\ & - (W'(c) - W'(\bar{c}) - W''(\bar{c})(c - \bar{c}))\nabla \cdot (\bar{c}\bar{\mathbf{u}}) \\ & - \left(\frac{1}{2}(c - \bar{c})^2 W''(\bar{c}) + \frac{1}{3}(c - \bar{c})^3 W'''(\bar{c}) + \frac{1}{4}(c - \bar{c})^4 \right) \nabla \cdot \bar{\mathbf{u}} \\ & + \left(\frac{1}{2}(c - \bar{c})^2 \nabla W''(\bar{c}) + \frac{1}{6}(c - \bar{c})^3 \nabla W'''(\bar{c}) \right) \cdot \bar{\mathbf{u}} \\ & - (c - \bar{c})(\mathbf{u} - \bar{\mathbf{u}}) \cdot \nabla W'(\bar{c}). \end{aligned} \quad (3.24)$$

The third term can be rewritten as follows,

$$\begin{aligned} I_3 = & \tau \left(W'(c) - W'(\bar{c}) - W''(\bar{c})(c - \bar{c}) - \frac{W'''(\bar{c})}{2}(c - \bar{c})^2 \right) \Delta(c - \bar{c}) \\ & + \tau W''(\bar{c})(c - \bar{c}) \Delta(c - \bar{c}) + \frac{W'''(\bar{c})}{2}(c - \bar{c})^2 \Delta(c - \bar{c}), \end{aligned} \quad (3.25)$$

i.e.,

$$\begin{aligned} I_3 = & \tau(c - \bar{c})^3 \Delta(c - \bar{c}) + \tau(3\bar{c}^2 - 1)(c - \bar{c}) \Delta(c - \bar{c}) + \tau 3\bar{c}(c - \bar{c})^2 \Delta(c - \bar{c}) \\ = & \nabla \cdot [\tau ((c - \bar{c})^3 + (3\bar{c}^2 - 1)(c - \bar{c}) + 3\bar{c}(c - \bar{c})^2) \nabla(c - \bar{c})] \\ & - 3\tau(c - \bar{c})^2 |\nabla(c - \bar{c})|^2 - 6\tau(c - \bar{c}) \nabla(c - \bar{c}) \cdot \nabla \bar{c} - \tau(3\bar{c}^2 - 1) |\nabla(c - \bar{c})|^2 \\ & - 3\tau(c - \bar{c})^2 \nabla(c - \bar{c}) \cdot \nabla \bar{c} - 6\tau\bar{c}(c - \bar{c}) |\nabla(c - \bar{c})|^2. \end{aligned} \quad (3.26)$$

Note that

$$-3\tau(c - \bar{c})^2 |\nabla(c - \bar{c})|^2 - \tau(3\bar{c}^2 - 1) |\nabla(c - \bar{c})|^2 - 6\tau\bar{c}(c - \bar{c}) |\nabla(c - \bar{c})|^2 \leq \tau |\nabla(c - \bar{c})|^2, \quad (3.27)$$

so that

$$\begin{aligned} I_3 \leq & \nabla \cdot [\tau ((c - \bar{c})^3 + (3\bar{c}^2 - 1)(c - \bar{c}) + 3\bar{c}(c - \bar{c})^2) \nabla(c - \bar{c})] \\ & - 6\tau(c - \bar{c}) \nabla(c - \bar{c}) \cdot \nabla \bar{c} - 3\tau(c - \bar{c})^2 \nabla(c - \bar{c}) \cdot \nabla \bar{c} + \tau |\nabla(c - \bar{c})|^2. \end{aligned} \quad (3.28)$$

Moving forward,

$$I_4 = -\nabla \cdot \left[\frac{1}{\beta}(c - \omega - (\bar{c} - \bar{\omega}))(\mathbf{c}\mathbf{u} - \bar{c}\bar{\mathbf{u}}) \right] + \frac{1}{\beta}(c - \bar{c})(\bar{\mathbf{u}} \cdot \nabla(c - \omega) - \mathbf{u} \cdot \nabla(\bar{c} - \bar{\omega})), \quad (3.29)$$

where

$$\frac{1}{\beta}(c - \bar{c})(\bar{\mathbf{u}} \cdot \nabla(c - \omega) - \mathbf{u} \cdot \nabla(\bar{c} - \bar{\omega})) = \frac{1}{\beta}(c - \bar{c})\bar{\mathbf{u}} \cdot \nabla(c - \omega - (\bar{c} - \bar{\omega})) - (c - \bar{c})(\mathbf{u} - \bar{\mathbf{u}}) \cdot \nabla(\bar{c} - \bar{\omega}), \quad (3.30)$$

and we write

$$\frac{1}{\beta}(c - \bar{c})\bar{\mathbf{u}} \cdot \nabla(c - \omega - (\bar{c} - \bar{\omega})) = \frac{1}{2\beta}\bar{\mathbf{u}} \cdot \nabla(c - \omega - (\bar{c} - \bar{\omega}))^2 + \frac{1}{\beta}(\omega - \bar{\omega})\bar{\mathbf{u}} \cdot \nabla(c - \omega - (\bar{c} - \bar{\omega})). \quad (3.31)$$

Furthermore, by the elliptic coupling, we have

$$\frac{1}{\beta}(\omega - \bar{\omega})\bar{\mathbf{u}} \cdot \nabla(c - \omega - (\bar{c} - \bar{\omega})) = -\gamma(\omega - \bar{\omega})\bar{\mathbf{u}} \cdot \nabla\Delta(\omega - \bar{\omega}) - (\omega - \bar{\omega})\bar{\mathbf{u}} \cdot \nabla\mathcal{R}_5. \quad (3.32)$$

Now, since for any scalar field φ and any vector field Φ ,

$$\begin{aligned} \varphi\Phi \cdot \nabla\Delta\varphi &= \nabla \cdot \left[\varphi\Delta\varphi\Phi - \nabla \cdot (\varphi\Phi)\nabla\varphi + \frac{|\nabla\varphi|^2}{2}\Phi \right] \\ &\quad + \frac{|\nabla\varphi|^2}{2}\nabla \cdot \Phi + (\nabla\varphi \otimes \nabla\varphi) : \nabla\Phi + \varphi\nabla\varphi \cdot \nabla(\nabla \cdot \Phi), \end{aligned} \quad (3.33)$$

we thereby obtain

$$\begin{aligned} I_4 &= -\nabla \cdot \left[\frac{1}{\beta}(c - \omega - (\bar{c} - \bar{\omega}))(c\mathbf{u} - \bar{c}\bar{\mathbf{u}}) - \frac{1}{2\beta}(c - \omega - (\bar{c} - \bar{\omega}))^2\bar{\mathbf{u}} \right] \\ &\quad + \nabla \cdot \left[\gamma(\omega - \bar{\omega})\Delta(\omega - \bar{\omega})\bar{\mathbf{u}} - \gamma\nabla \cdot ((\omega - \bar{\omega})\bar{\mathbf{u}})\nabla(\omega - \bar{\omega}) + \gamma\frac{|\nabla(\omega - \bar{\omega})|^2}{2}\bar{\mathbf{u}} \right] \\ &\quad - (c - \bar{c})(\mathbf{u} - \bar{\mathbf{u}}) \cdot \nabla(\bar{c} - \bar{\omega}) - \frac{1}{2\beta}(c - \omega - (\bar{c} - \bar{\omega}))^2\nabla \cdot \bar{\mathbf{u}} - (\omega - \bar{\omega})\bar{\mathbf{u}} \cdot \nabla\mathcal{R}_5 \\ &\quad + \gamma\frac{|\nabla(\omega - \bar{\omega})|^2}{2}\nabla \cdot \bar{\mathbf{u}} + \gamma(\nabla(\omega - \bar{\omega}) \otimes \nabla(\omega - \bar{\omega})) : \nabla\bar{\mathbf{u}} + \gamma(\omega - \bar{\omega})\nabla(\omega - \bar{\omega}) \cdot \nabla(\nabla \cdot \bar{\mathbf{u}}). \end{aligned} \quad (3.34)$$

Finally, the convective terms in the relative energy balance (3.16) amount to

$$\begin{aligned} &-[(\mathbf{u} \cdot \nabla)\mathbf{u} - (\bar{\mathbf{u}} \cdot \nabla)\bar{\mathbf{u}}] \cdot (\mathbf{u} - \bar{\mathbf{u}}) - \frac{1}{2}[(\nabla \cdot \mathbf{u})\mathbf{u} - (\nabla \cdot \bar{\mathbf{u}})\bar{\mathbf{u}}] \cdot (\mathbf{u} - \bar{\mathbf{u}}) \\ &= -\nabla \cdot \left[\frac{|\mathbf{u} - \bar{\mathbf{u}}|^2}{2}\mathbf{u} \right] - ((\mathbf{u} - \bar{\mathbf{u}}) \cdot \nabla)\bar{\mathbf{u}} \cdot (\mathbf{u} - \bar{\mathbf{u}}) - \frac{1}{2}(\nabla \cdot (\mathbf{u} - \bar{\mathbf{u}}))\bar{\mathbf{u}} \cdot (\mathbf{u} - \bar{\mathbf{u}}). \end{aligned} \quad (3.35)$$

The proof can be completed by adding (3.21), (3.24), (3.28), (3.34) and (3.35). \square

Remark 3.5 Since the terms $(c - \bar{c})^4$ and $(c - \bar{c})^2$ are controlled by definition of the reduced relative energy, we can simply use Young's inequality to handle the cubic term $(c - \bar{c})^3$.

Remark 3.6 Note that the integral of the term $\gamma(\omega - \bar{\omega})\nabla(\omega - \bar{\omega}) \cdot \nabla(\nabla \cdot \bar{\mathbf{u}})$ in (3.15) can be controlled by a multiple of the integral of the reduced relative entropy without resorting to Poincaré's inequality, since

$$(\omega - \bar{\omega})^2 \leq \frac{1}{2\beta}(\omega - \bar{\omega})^2 + \frac{\beta}{2}(c - \omega - (\bar{c} - \bar{\omega}))^2 + \frac{1}{2}(\omega - \bar{\omega})^2 + \frac{1}{2}(c - \bar{c})^2,$$

so that

$$\frac{1}{2}(\omega - \bar{\omega})^2 \leq \frac{1}{2\beta}(\omega - \bar{\omega})^2 + \frac{\beta}{2}(c - \omega - (\bar{c} - \bar{\omega}))^2 + \frac{1}{2}(c - \bar{c})^2.$$

To control the growth rate of the reduced relative entropy η^ε , we recall (3.14). Our next step is to compute the rate of $(c - \bar{c})^2$. Note that this term is nonlinear in the weak solution \mathbf{U} and, in particular, not controlled in the energy inequality (3.4). This means that some care is needed to carry it out without resorting to classical solutions \mathbf{U} .

Proposition 3.7 Let \mathbf{U} be a weak solution to (2.7) and $\bar{\mathbf{U}}$ be a classical solution to (3.1). Then, for every $t \leq T$ there holds

$$\begin{aligned} \int_{\Omega} \frac{(c - \bar{c})^2}{2}(t, \mathbf{x}) d\mathbf{x} &= \int_{\Omega} \frac{(c - \bar{c})^2}{2}(0, \mathbf{x}) d\mathbf{x} + \int_0^t \int_{\Omega} -\tau|\nabla(c - \bar{c})|^2 - \frac{1}{2}(c - \bar{c})^2\nabla \cdot (\mathbf{u} - \bar{\mathbf{u}}) \\ &\quad - (c - \bar{c})(\mathbf{u} - \bar{\mathbf{u}}) \cdot \nabla\bar{c} - \bar{c}(c - \bar{c})\nabla \cdot (\mathbf{u} - \bar{\mathbf{u}}) - \frac{1}{2}(c - \bar{c})^2\nabla \cdot \bar{\mathbf{u}} \\ &\quad - (c - \omega - (\bar{c} - \bar{\omega}))\nabla \cdot (\mathbf{v} - \bar{\mathbf{v}}) + (\mathbf{v} - \bar{\mathbf{v}})\nabla(\omega - \bar{\omega}) + \mathcal{R}_3(c - \bar{c}) d\mathbf{x} ds. \end{aligned} \quad (3.36)$$

Proof: First we note that, by testing the evolution equation for c with $\varphi \in C_c^\infty((0, T) \times \Omega)$, it is evident that $c \in H^1((0, T); H^{-1}(\Omega))$. Thus, it follows that for any $\psi \in C_c^\infty((0, T) \times \Omega)$, $\psi \geq 0$, there holds

$$\int_0^T \int_\Omega \frac{(c - \bar{c})^2}{2} \psi_t \, d\mathbf{x} dt = - \int_0^T \langle c_t - \bar{c}_t, (c - \bar{c})\psi \rangle_{H^{-1}(\Omega), H^1(\Omega)} \, dt, \quad (3.37)$$

which allows us to use the evolution equation of $c - \bar{c}$ directly, i.e.,

$$\begin{aligned} - \int_0^T \langle (c_t - \bar{c}_t), (c - \bar{c})\psi \rangle_{H^{-1}(\Omega), H^1(\Omega)} \, dt &= \int_0^T \int_\Omega \psi(c - \bar{c}) \nabla \cdot (c\mathbf{u} - \bar{c}\bar{\mathbf{u}}) + \psi(c - \bar{c}) \nabla \cdot (\mathbf{v} - \bar{\mathbf{v}}) \\ &\quad - \tau \nabla(c - \bar{c}) \cdot \nabla(\psi(c - \bar{c})) - \psi \mathcal{R}_3(c - \bar{c}) \, d\mathbf{x} dt. \end{aligned} \quad (3.38)$$

Now, on the one hand

$$\begin{aligned} \psi(c - \bar{c}) \nabla \cdot (c\mathbf{u} - \bar{c}\bar{\mathbf{u}}) &= \psi(c - \bar{c}) \nabla \cdot ((c - \bar{c})(\mathbf{u} - \bar{\mathbf{u}}) + (c - \bar{c})\bar{\mathbf{u}} + \bar{c}(\mathbf{u} - \bar{\mathbf{u}})) \\ &= \nabla \cdot \left[\psi \frac{(c - \bar{c})^2}{2} \mathbf{u} \right] + \psi \frac{(c - \bar{c})^2}{2} \nabla \cdot (\mathbf{u} - \bar{\mathbf{u}}) - \frac{(c - \bar{c})^2}{2} (\mathbf{u} - \bar{\mathbf{u}}) \cdot \nabla \psi \\ &\quad + \psi \frac{(c - \bar{c})^2}{2} \bar{\mathbf{u}} - \frac{(c - \bar{c})^2}{2} \bar{\mathbf{u}} \cdot \nabla \psi + \psi(c - \bar{c}) ((\mathbf{u} - \bar{\mathbf{u}}) \cdot \nabla \bar{c} + \bar{c} \nabla \cdot (\mathbf{u} - \bar{\mathbf{u}})), \end{aligned} \quad (3.39)$$

while

$$\begin{aligned} \psi(c - \bar{c}) \nabla \cdot (\mathbf{v} - \bar{\mathbf{v}}) &= \psi(\omega - \bar{\omega}) \nabla \cdot (\mathbf{v} - \bar{\mathbf{v}}) + \psi(c - \omega - (\bar{c} - \bar{\omega})) \nabla \cdot (\mathbf{v} - \bar{\mathbf{v}}) \\ &= \nabla \cdot [\psi(\omega - \bar{\omega})(\mathbf{v} - \bar{\mathbf{v}})] - (\omega - \bar{\omega})(\mathbf{v} - \bar{\mathbf{v}}) \cdot \nabla \psi - \psi(\mathbf{v} - \bar{\mathbf{v}}) \cdot \nabla(\omega - \bar{\omega}). \end{aligned} \quad (3.40)$$

Using the above identities, we thus obtain (3.36) by an approximation $\psi \rightarrow \mathbb{1}_{[0, T] \times \Omega}$. \square

Now, we can, after carefully bounding the terms in (3.15) and (3.36) and by using damping and bulk viscosity, apply Gronwall's lemma to the relative entropy between \mathbf{U} and $\bar{\mathbf{U}}$.

Lemma 3.8 (Bound for the growth rate of the reduced relative energy) *Let \mathbf{U} be a weak solution to (2.7) and let $\bar{\mathbf{U}}$ be a classical solution to (3.1). Let $\varepsilon \in (0, 1)^4$, $\tau \lesssim \beta \lesssim \delta$ and assume that $\bar{c} \in L^\infty((0, T) \times \Omega)$, uniformly in ε . Then there holds for all $t \leq T$,*

$$\begin{aligned} \int_\Omega \eta^\varepsilon(\mathbf{U}, \bar{\mathbf{U}})(t, \mathbf{x}) \, d\mathbf{x} &\leq \int_\Omega \eta^\varepsilon(\mathbf{U}, \bar{\mathbf{U}})(0, \mathbf{x}) \, d\mathbf{x} + \int_0^t K \int_\Omega \eta^\varepsilon(\mathbf{U}, \bar{\mathbf{U}})(s, \mathbf{x}) \, d\mathbf{x} + \int_\Omega \mathcal{R} \, d\mathbf{x} \\ &\quad - \nu |\mathbf{u} - \bar{\mathbf{u}}|_{H^1(\Omega)}^2 - \frac{(\lambda + \nu)}{2} \|\nabla \cdot (\mathbf{u} - \bar{\mathbf{u}})\|_{L^2(\Omega)}^2 - \frac{1}{2} \|\mathbf{v} - \bar{\mathbf{v}}\|_{L^2(\Omega)}^2 \\ &\quad - \frac{\delta}{2} \|\nabla \cdot (\mathbf{v} - \bar{\mathbf{v}})\|_{L^2(\Omega)}^2 - \frac{\tau}{2\beta} \|\nabla(c - \bar{c})\|_{L^2(\Omega)}^2 \, ds, \end{aligned} \quad (3.41)$$

with the remainder

$$\begin{aligned} \mathcal{R} &:= \alpha \mathcal{R}_1(p - \bar{p}) + \mathcal{R}_2(\mathbf{u} - \bar{\mathbf{u}}) + \frac{1}{\beta} \mathcal{R}_3(c - \omega - (\bar{c} - \bar{\omega})) + \delta \mathcal{R}_4(\mathbf{v} - \bar{\mathbf{v}}) \\ &\quad + \mathcal{R}_5(\omega_t - \bar{\omega}_t) + \mathcal{R}_3(W''(\bar{c}) + 1)(c - \bar{c}), \end{aligned} \quad (3.42)$$

and where the constant K is such that,

$$\begin{aligned} K &\lesssim (\lambda + \nu)^{-1} + \gamma^{-1} + \|\nabla \cdot (\bar{c}\bar{\mathbf{u}} + \bar{\mathbf{v}})\|_\infty + \|\bar{\mathbf{u}}\|_\infty^2 + \|\nabla \cdot \bar{\mathbf{u}}\|_\infty + \|\nabla \bar{\mathbf{u}} + \nabla \bar{\mathbf{u}}^\top\|_\infty \\ &\quad + \|\nabla \bar{c}\|_\infty + \|\bar{\mathbf{u}} \cdot \nabla \bar{c}\|_\infty + \beta \gamma \|\nabla \Delta \bar{\omega}\|_\infty. \end{aligned} \quad (3.43)$$

Remark 3.9 The a-priori assumption $\bar{c} \in L^\infty(0, T; \Omega)$ is used to simply bound $\|W''(\bar{c})\|_\infty$ and $\|W'''(\bar{c})\|_\infty$, uniformly in ε , and thus conveniently omit these prefactors in the description of K .

Remark 3.10 Only bulk viscosity has been used to absorb problematic terms. As such, Lemma 3.8 holds even in the case of vanishing shear viscosity, $\nu = 0$, as long as $\lambda > 0$ which only appears in the approximating system anyhow. This is reflected in the scaling of the constant K in (3.43).

We will now derive an a-priori error estimate of the difference between a solution to (2.7) and a solution to (2.1) via Lemma 3.8. To this end, we have to construct a suitable solution $\bar{\mathbf{U}}$ to (3.1) from the exact solution to the NSCH system (2.1).

Remark 3.11 Note that if $\bar{\mathbf{U}}$ is chosen straightforwardly, the resulting convergence rate is reduced. Indeed, setting $\bar{p} := \tilde{p}$ and $\bar{\mathbf{u}} = \tilde{\mathbf{u}}$ with $(\tilde{p}, \tilde{\mathbf{u}}, \tilde{c})$ the exact solution to the NSCH system (2.1) would yield $\mathcal{R}_1 = -\tilde{p}_t$. This would lead to a convergence rate of order $1/2$ in α due to the term $\alpha\mathcal{R}_1(p - \bar{p})$ in (3.15) and the fact that the relative energy only controls $\alpha(p - \tilde{p})^2$, i.e., the control vanishes in the $\alpha \rightarrow 0$ limit.

Instead, we do the following.

Proposition 3.12 Let $\varepsilon \in (0, 1)^4$ and $\tau \lesssim \beta \lesssim \delta$. Let $(\tilde{p}, \tilde{\mathbf{u}}, \tilde{c})$ denote a classical solution of the NSCH system (2.1) and let $\theta : (0, T) \times \Omega \rightarrow \mathbb{R}$ satisfy

$$\Delta\theta(t, \cdot) = \tilde{p}_t(t, \cdot), \quad (3.44)$$

and $\int_{\Omega} \theta(t, \cdot) \, d\mathbf{x} = 0$ for almost all $t \in (0, T)$. Set

$$\bar{p} := \tilde{p}, \quad \bar{\mathbf{u}} := \tilde{\mathbf{u}} - \alpha\nabla\theta, \quad \bar{c} := \tilde{c}, \quad \bar{\mathbf{v}} := -\nabla\mu(\tilde{c}) + \alpha\tilde{c}\nabla\theta + \tau\nabla\tilde{c}, \quad (3.45)$$

and choose $\bar{\omega}$ as the solution to

$$-\gamma\Delta\bar{\omega} + \frac{1}{\beta}\bar{\omega} = \frac{1}{\beta}\tilde{c}. \quad (3.46)$$

Let \mathbf{U} be a weak solution to (2.7) and let $\bar{\mathbf{U}}$ be defined by (3.45)-(3.46). Then, there exist constants $K, k, C > 0$ such that for all times $t \leq T$, there holds

$$\begin{aligned} \int_{\Omega} \eta^{\varepsilon}(t, \mathbf{x}) \, d\mathbf{x} &\leq \int_{\Omega} \eta^{\varepsilon}(0, \mathbf{x}) \, d\mathbf{x} + \int_0^t K \int_{\Omega} \eta^{\varepsilon}(s, \mathbf{x}) \, d\mathbf{x} + C\alpha^2 \|\tilde{p}_t\|_{H^1}^2 (\|\tilde{\mathbf{u}}\|_{H^1}^2 + \alpha^2 \|\tilde{p}_t\|_{L^2}^2) \\ &\quad + C\alpha^2 \|\tilde{p}_t\|_{L^2}^2 (\|\tilde{\mathbf{u}}\|_{\infty}^2 + \alpha^2 \|\tilde{p}_t\|_{H^1}^2 + k(\lambda + \nu) + k\|\tilde{c}\|_{\infty}^2) + C\alpha^2 \nu \|\tilde{p}_t\|_{H^1}^2 \\ &\quad + \beta^2 \gamma^2 \left(\left(\frac{k\|\tilde{c}\|_{\infty}^2}{\lambda + \nu} + \|\nabla\tilde{c}\|_{\infty}^2 \right) |\tilde{c}|_{H^4}^2 + |\tilde{c}|_{H^5}^2 \right) + C \frac{k\alpha^2}{(\lambda + \nu)} \|\tilde{p}_{tt}\|_{L^2}^2 \\ &\quad + k\delta^2 (|\mu(\tilde{c})_t|_{H^1}^2 + \tau^2 |\tilde{c}_t|_{H^1}^2 + \tau^2 |\tilde{c}|_{H^3}^2 + |\mu(\tilde{c})|_{H^3}^2 + C\alpha^2 \|\nabla\tilde{c}\|_{\infty}^2 \|\tilde{p}_t\|_{L^2}^2) \\ &\quad + Ck\alpha^2 \delta^2 (|\tilde{p}_t|_{H^1}^2 (|\tilde{c}|_{H^2}^2 + \|\tilde{c}\|_{L^2}^2) + \|\tilde{c}\|_{\infty}^2 (|\tilde{p}_t|_{H^1}^2 + \|\tilde{p}_{tt}\|_{L^2}^2)) + Ck\tau^2 |\tilde{c}|_{H^1}^2 ds. \end{aligned} \quad (3.47)$$

The constant $K > 0$ is as in (3.43), $k > 0$ is large enough to facilitate certain Young's inequalities and $C > 0$ is a constant coming from elliptic estimates and Sobolev inequalities.

Proof: By definition, $(\bar{p}, \bar{\mathbf{u}}, \bar{c}, \bar{\mathbf{v}}, \bar{\omega})$ is a solution to (3.1) with residuals

$$\mathcal{R}_1 := 0,$$

$$\mathcal{R}_2 := \alpha\nabla\theta_t + \alpha(\tilde{\mathbf{u}} \cdot \nabla)\nabla\theta + \alpha(\nabla\theta \cdot \nabla)\tilde{\mathbf{u}} + \frac{\alpha}{2}\bar{\mathbf{u}}\Delta\theta - \alpha\nu\Delta\nabla\theta - \alpha(\lambda + \nu)\nabla\Delta\theta + \gamma\bar{c}\nabla\Delta(\bar{c} - \bar{\omega}),$$

$$\mathcal{R}_3 := 0,$$

$$\mathcal{R}_4 := -\bar{\mathbf{v}}_t - \frac{\gamma}{\delta}\nabla\Delta(\bar{c} - \bar{\omega}) - \frac{\alpha}{\delta}\bar{c}\nabla\theta - \frac{\tau}{\delta}\nabla\bar{c} - \nabla(\nabla \cdot \bar{\mathbf{v}}),$$

$$\mathcal{R}_5 := 0.$$

We start from (3.15) and note that the contribution of the second residual can be bounded as follows:

$$\begin{aligned} \int_{\Omega} \mathcal{R}_2(\mathbf{u} - \bar{\mathbf{u}}) \, d\mathbf{x} &= \int_{\Omega} -\alpha\theta_t \nabla \cdot (\mathbf{u} - \bar{\mathbf{u}}) - \alpha(\tilde{\mathbf{u}} \cdot \nabla)\nabla\theta \cdot (\mathbf{u} - \bar{\mathbf{u}}) - \alpha(\nabla\theta \cdot \nabla)\bar{\mathbf{u}} \cdot (\mathbf{u} - \bar{\mathbf{u}}) \\ &\quad - \frac{\alpha}{2}\bar{\mathbf{u}} \cdot (\mathbf{u} - \bar{\mathbf{u}})\Delta\theta + \alpha\nu\Delta\nabla\theta \cdot (\mathbf{u} - \bar{\mathbf{u}}) + \alpha(\lambda + \nu)(\nabla \cdot (\mathbf{u} - \bar{\mathbf{u}}))\Delta\theta \\ &\quad - \gamma(\bar{c}\Delta(\bar{c} - \bar{\omega}))\nabla \cdot (\mathbf{u} - \bar{\mathbf{u}}) - \gamma(\nabla\bar{c} \cdot (\mathbf{u} - \bar{\mathbf{u}}))\Delta(\bar{c} - \bar{\omega}) \, d\mathbf{x} \\ &\leq \frac{k\alpha^2}{2(\lambda + \nu)} \|\theta_t\|_{L^2}^2 + \frac{\lambda + \nu}{2k} \|\nabla \cdot (\mathbf{u} - \bar{\mathbf{u}})\|_{L^2}^2 + \frac{\alpha^2}{2} \|\tilde{\mathbf{u}}\|_{\infty}^2 |\theta|_{H^2}^2 + \frac{1}{2} \|\mathbf{u} - \bar{\mathbf{u}}\|_{L^2}^2 \\ &\quad + \frac{\alpha^2}{2} \|\nabla\theta\|_{\infty}^2 \|\bar{\mathbf{u}}\|_{H^1}^2 + \frac{1}{2} \|\mathbf{u} - \bar{\mathbf{u}}\|_{L^2}^2 + \frac{\alpha^2}{4} \|\bar{\mathbf{u}}\|_{\infty}^2 |\theta|_{H^2}^2 + \frac{1}{4} \|\mathbf{u} - \bar{\mathbf{u}}\|_{L^2}^2 \\ &\quad + \frac{\alpha^2\nu}{2} |\theta|_{H^3}^2 + \frac{\nu}{2} \|\mathbf{u} - \bar{\mathbf{u}}\|_{L^2}^2 + \frac{k\alpha^2(\lambda + \nu)}{2} |\theta|_{H^2}^2 + \frac{\lambda + \nu}{2k} \|\nabla \cdot (\mathbf{u} - \bar{\mathbf{u}})\|_{L^2}^2 \\ &\quad + \frac{k\gamma^2}{2(\lambda + \nu)} \|\bar{c}\|_{\infty}^2 |\bar{c} - \bar{\omega}|_{H^2}^2 + \frac{\lambda + \nu}{2k} \|\nabla \cdot (\mathbf{u} - \bar{\mathbf{u}})\|_{L^2}^2 + \frac{\gamma^2}{2} \|\nabla\bar{c}\|_{\infty}^2 |\bar{c} - \bar{\omega}|_{H^2}^2 \\ &\quad + \frac{1}{2} \|\mathbf{u} - \bar{\mathbf{u}}\|_{L^2}^2, \end{aligned} \quad (3.48)$$

where choosing $k > 0$ large enough allows for absorption of the divergence terms via bulk viscosity.

The other residual is bounded as follows,

$$\begin{aligned} \int_{\Omega} \delta \mathcal{R}_4(\mathbf{v} - \bar{\mathbf{v}}) d\mathbf{x} &\leq \frac{k\delta^2}{2} \|\bar{\mathbf{v}}_t\|_{L^2}^2 + \frac{k\gamma^2}{2} |\bar{c} - \bar{\omega}|_{H^3}^2 + \frac{k\alpha^2}{2} |\bar{c}|_{\infty}^2 |\theta|_{H^1}^2 \\ &\quad + \frac{k\tau^2}{2} |\bar{c}|_{H^1}^2 + \frac{k\delta^2}{2} |\bar{\mathbf{v}}|_{H^2}^2 + \frac{5}{2k} \|\mathbf{v} - \bar{\mathbf{v}}\|_{L^2}^2, \end{aligned} \quad (3.49)$$

where choosing $k > 0$ large enough allows for absorption of the $\|\mathbf{v} - \bar{\mathbf{v}}\|_{L^2}^2$ terms via damping.

It remains to apply the elliptic estimates

$$|\bar{c} - \bar{w}|_{H^2(\Omega)}^2 \leq \beta^2 |\bar{c}|_{H^4(\Omega)}^2, \quad |\bar{c} - \bar{w}|_{H^3(\Omega)}^2 \leq \beta^2 |\bar{c}|_{H^5(\Omega)}^2, \quad (3.50)$$

that can be found in [19], and to note that on the one hand

$$\|\theta_t\|_{L^2} \lesssim \|\tilde{p}_{tt}\|_{L^2}, \quad (3.51)$$

while for $s > 1/2$, one has the bound

$$\|\nabla \theta\|_{\infty} \lesssim \|\theta\|_{H^{2+s}} \lesssim \|\tilde{p}_t\|_{H^s}, \quad (3.52)$$

by Sobolev embedding and elliptic estimates. \square

Finally, we obtain the following a-priori error estimate.

Theorem 3.13 *Let $\varepsilon \in (0, 1)^4$, $\tau \lesssim \beta \lesssim \delta$, and \mathbf{U} denote a weak solution to (2.7). Let $(\tilde{p}, \tilde{\mathbf{u}}, \tilde{c})$ denote a classical solution to the NSCH system (2.1) complemented with periodic boundary conditions, such that*

$$\tilde{p} \in C^1([0, T]; H^2(\Omega)) \cap C^2([0, T]; L^2(\Omega)), \quad (3.53)$$

$$\tilde{\mathbf{u}}, |\nabla \tilde{\mathbf{u}} + \nabla \tilde{\mathbf{u}}^T|_F \in L^\infty((0, T) \times \Omega), \quad (3.54)$$

$$\tilde{c} \in L^\infty(0, T; W^{4,\infty}(\Omega)) \cap L^\infty(0, T; H^5(\Omega)) \cap C^1([0, T]; H^3(\Omega)), \quad (3.55)$$

and choose $\tilde{\omega}$ as the solution to (3.46) with periodic boundary conditions.

Then, under the initial conditions

$$p(0, \cdot) = \tilde{p}(0, \cdot) \in H^1(\Omega), \quad \mathbf{u}(0, \cdot) = \tilde{\mathbf{u}}(0, \cdot) \in W^{1,\infty}(\Omega; \mathbb{R}^d), \quad (3.56)$$

$$c(0, \cdot) = \tilde{c}(0, \cdot) \in W^{4,\infty}(\Omega) \cap H^5(\Omega), \quad \mathbf{v}(0, \cdot) = -\nabla \mu(c(0, \cdot)), \quad (3.57)$$

there holds for all times $t \in (0, T)$,

$$\begin{aligned} &\left(\sqrt{\alpha} \|p - \tilde{p}\| + \|c - \tilde{c}\| + \|(c - \tilde{c})^2\| + \sqrt{\beta} \left\| \frac{c - \omega}{\beta} + \gamma \Delta \tilde{c} \right\| \right. \\ &\quad \left. + \|\mathbf{u} - \tilde{\mathbf{u}}\| + \sqrt{\delta} \|\mathbf{v} + \nabla \mu(\tilde{c})\| + \sqrt{\gamma} \|\nabla \omega - \nabla \tilde{c}\| \right) (t) \\ &\leq C \exp(tK) \left(\frac{1}{K} \left[\left(\frac{\alpha + \beta \gamma}{\sqrt{\lambda + \nu}} + \delta \right) + \alpha + \tau \right] + \alpha + \beta + \tau \right) < \infty. \end{aligned} \quad (3.58)$$

with $\|\cdot\| := \|\cdot\|_{L^2(\Omega)}$, and where $K > 0$ is as in (3.43) and the constant $C > 0$ depends solely on the norms (3.54)-(3.53) of the solution $[\tilde{\mathbf{u}}, \tilde{c}, \tilde{p}]$ to the NSCH system (2.1).

Proof: The proof is a mere application of Gronwall's Lemma to (3.47) in the context of Proposition 3.12 since, indeed, the left-hand side of (3.58) is bounded by a multiple of $\sqrt{\eta^\varepsilon(\mathbf{U}, \bar{\mathbf{U}})} + \alpha + \beta + \tau$ with $\bar{\mathbf{U}}$ as defined in Proposition 3.12 due to the regularity assumptions (3.54)-(3.53). Furthermore, note that K as defined in (3.43) is independent of ε since, by definition, the relaxation parameters are bounded from above. \square

Remark 3.14 *From (3.58) it is evident that the relaxation system provides approximations of the pressure, the Laplacian of the phase field variable and the gradient of the chemical potential of the target system as*

$$\|p - \tilde{p}\|_{L^\infty L^2} \leq C_0 \sqrt{\alpha}, \quad \text{if } \delta \lesssim \alpha, \quad (3.59)$$

$$\left\| \frac{c - \omega}{\beta} + \gamma \Delta \tilde{c} \right\|_{L^\infty L^2} \leq C_0 \sqrt{\beta}, \quad \text{if } \alpha, \delta \lesssim \beta, \quad (3.60)$$

$$\|\mathbf{v} + \nabla \mu(\tilde{c})\|_{L^\infty L^2} \leq C_0 \sqrt{\delta}, \quad \text{if } \alpha \lesssim \delta, \quad (3.61)$$

where the constant C_0 depends on T, γ, λ, ν and norms of the target solution as specified in Theorem 3.13.

Remark 3.15 (Convergence in physical domains) *By similar considerations, a convergence result in the spirit of Theorem 3.13 can be proven in physical domains with convergence order $O(\alpha^{1/2} + \beta + \delta + \tau)$. The sub-optimal rate in α is due to a difficulty that arises via the no-flux boundary conditions for $\bar{\mathbf{u}}$. Using the same strategy as in the proof of (3.47) does not work in this case since additional residual terms appear that are concentrated on the boundary and cannot be absorbed.*

Remark 3.16 (Euler-Cahn-Hilliard) *Let us stress that Theorem 3.13 remains valid in the inviscid regime $\nu = 0$, as long as $\lambda > 0$. Even more so, in the context of an Euler-Cahn-Hilliard system (i.e., referring to (2.1) with $\nu = 0$), the $O(\alpha + \beta + \delta + \tau)$ convergence result can be generalized to physical domains if the impermeability condition $\mathbf{u} \cdot \mathbf{n} = 0$ for the velocity fields is prescribed on the boundary. This result is validated by numerical tests in Section 4.*

4. Numerical justification of the relaxation approximation

In this section, we first introduce tailored finite-difference methods for the NSCH system and the relaxation approximations. Then, numerical experiments are presented that confirm the convergence result from Theorem 3.13 obtained in Section 3. For this, simulations in one and two spatial dimensions are performed with a variety of initial data including a single droplet which relaxes into its equilibrium, the Ostwald ripening of two bubbles, the merging of two bubbles and a droplet-wall interaction. Besides the convergence of the relaxation formulation of the NSCH system (2.7) to the original NSCH system (2.1) for $|\varepsilon| \rightarrow 0$, the effect of the grid resolution and time step size on this convergence is investigated. However, only the inviscid limit systems of (2.1) and (2.7) with $\nu = 0$ are considered numerically. The structure of this section is as follows: First, in Sections 4.1.1, 4.1.2, the numerical discretization of the original NSCH system (2.1) and its relaxation formulation (2.7) are outlined, respectively. This is followed by numerical experiments in one dimension which are utilized to investigate the convergence of (2.7) to (2.1) for $|\varepsilon| \rightarrow 0$. In Section 4.2, beyond the convergence for $|\varepsilon| \rightarrow 0$ at a fixed grid resolution and time step size, its sensitivity with respect to the grid resolution and time step size is examined. Finally, in Section 4.3, two-dimensional convergence results are presented.

4.1. A numerical approach for the NSCH system and the relaxation approximation

4.1.1. A finite-difference MAC method for the NSCH system

For the numerical discretization of NSCH system (2.1), a second-order accurate conservative finite-difference scheme in space is utilized following ideas from [13, 39]. Advancement in time is realized by the use of a first-order accurate implicit method and a constant time step size Δt . For this, the domain $\Omega = (x_{min}, x_{max}) \times (y_{min}, y_{max})$ is tessellated into a Cartesian equispaced marker-and-cell (MAC) grid with $N = N_x \times N_y$ elements. Each element $\Omega_{i,j}$ has a volume given as $\text{vol}(\Omega_{i,j}) = \Delta x \Delta y$ with $i = 1, \dots, N_x$ and $j = 1, \dots, N_y$. The length of the cell edges in the x - and y -direction are defined as $\Delta x = \frac{x_{max} - x_{min}}{N_x}$ and $\Delta y = \frac{y_{max} - y_{min}}{N_y}$, respectively. As common for a MAC grid, the *thermodynamic* variables, i.e. the phase field variable c and the pressure p , are defined at the cell centers $\mathbf{x}_{i,j} = (x_i, y_j)$ of each element $\Omega_{i,j}$. In contrast, the *hydrodynamic* variables which means the velocities in the x and y -directions, $\mathbf{u} = (u_1, u_2)$, are defined on a staggered grid with the cell centers of these corresponding elements $\Omega_{i-\frac{1}{2},j}$ and $\Omega_{i,j-\frac{1}{2}}$ defined on the edges of the elements $\Omega_{i,j}$, see Fig. 1a for a graphical illustration.

The semi-discretization of the governing equations (2.1) in time reads as

$$c^* + \Delta t \left[\nabla \cdot (c^* \mathbf{u}^n) - \nabla \cdot (W''(c^n) \nabla c^* - \gamma \nabla \Delta c^*) \right] = c^n, \quad (4.1a)$$

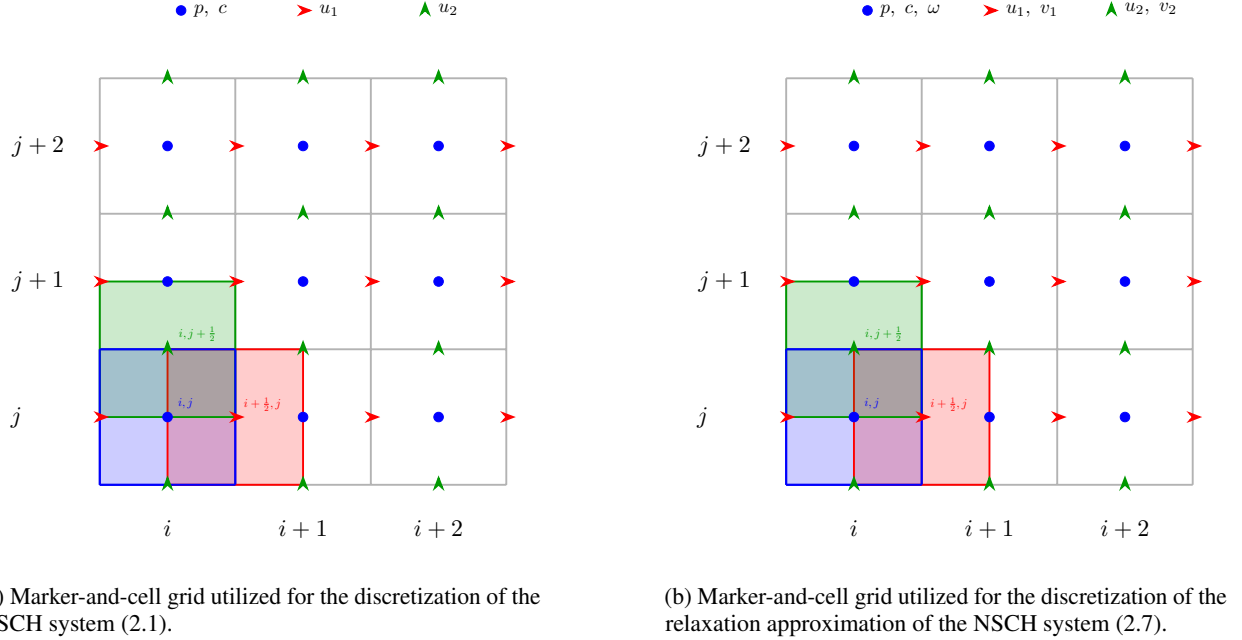
$$\mathbf{u}^* + \Delta t \nabla \cdot (\mathbf{u}^* \otimes \mathbf{u}^n) = \mathbf{u}^n - \Delta t c^* \left[W''(c^n) \nabla c^* - \gamma \nabla \Delta c^* \right], \quad (4.1b)$$

$$\Delta t \Delta p^{n+1} = \nabla \cdot \mathbf{u}^*, \quad (4.1c)$$

$$\mathbf{u}^{n+1} = \mathbf{u}^* - \Delta t \nabla \cdot p^{n+1}, \quad (4.1d)$$

$$c^{n+1} + \Delta t \left[\nabla \cdot (c \mathbf{u})^{n+1} - \nabla \cdot (W''(c^*) \nabla c^{n+1} - \gamma \nabla \Delta c^{n+1}) \right] = c^n. \quad (4.1e)$$

The scheme in (4.1) is a straightforward extension of a classical second-order accurate semi-implicit conservative finite-difference scheme for the inviscid case, i.e., (2.1) with $\nu = 0$. Herein, the projection method proposed in [9] which is based on a Helmholtz-Hodge decomposition of the velocity field is used in (4.1c) and (4.1d) to guarantee the divergence-free condition of the velocity field. Due to the semi-implicit discretization, the equations in (4.1) can be solved independently in the order as they appear in each time step. Moreover, for each solution variable only a linear system has to be solved which can be easily realized by the use of the GMRES algorithm [37]. A detailed discussion of the utilized stencils for the approximation of the spatial derivatives in (4.1) is given in the Appendix A.



(a) Marker-and-cell grid utilized for the discretization of the NSCH system (2.1).

(b) Marker-and-cell grid utilized for the discretization of the relaxation approximation of the NSCH system (2.7).

Figure 1: Comparison of the spatial distribution of the solution variables for the NSCH system (2.1) and its relaxation approximation(2.7).

4.1.2. A finite-difference MAC method for the relaxation approximation

Similar to the discretization of the original NSCH system, also for the relaxation formulation of the NSCH system, a second-order accurate semi-implicit conservative finite-difference scheme is used. However, as outlined in Section 2.2, system (2.7) has several modifications in comparison to the relaxation formulation originally proposed in [30]. In order to demonstrate that the convergence result of Theorem 3.13 can be numerically reproduced also without these modifications, the relaxation formulation as proposed in [30] is considered in the following. Consequently, the investigated system is given as

$$\begin{aligned}
 p_t^{\tilde{\varepsilon}} + \frac{1}{\alpha} \nabla \cdot \mathbf{u}^{\tilde{\varepsilon}} &= 0, \\
 \mathbf{u}_t^{\tilde{\varepsilon}} + (\mathbf{u}^{\tilde{\varepsilon}} \cdot \nabla) \mathbf{u}^{\tilde{\varepsilon}} + \frac{1}{2} (\nabla \cdot \mathbf{u}^{\tilde{\varepsilon}}) \mathbf{u}^{\tilde{\varepsilon}} + \nabla p^{\tilde{\varepsilon}} &= -c^{\tilde{\varepsilon}} \nabla \left(W'(c^{\tilde{\varepsilon}}) + \frac{1}{\beta} (c^{\tilde{\varepsilon}} - \omega^{\tilde{\varepsilon}}) \right), \\
 c_t^{\tilde{\varepsilon}} + \nabla \cdot (c^{\tilde{\varepsilon}} \mathbf{u}^{\tilde{\varepsilon}}) + \nabla \cdot \mathbf{v}^{\tilde{\varepsilon}} &= 0, \\
 \mathbf{v}_t^{\tilde{\varepsilon}} + \frac{1}{\delta} \nabla \left(W'(c^{\tilde{\varepsilon}}) + \frac{1}{\beta} c^{\tilde{\varepsilon}} \right) &= -\frac{\mathbf{v}^{\tilde{\varepsilon}}}{\delta} + \frac{1}{\delta \beta} \nabla \omega^{\tilde{\varepsilon}}, \\
 -\gamma \Delta \omega^{\tilde{\varepsilon}} + \frac{1}{\beta} \omega^{\tilde{\varepsilon}} &= \frac{1}{\beta} c^{\tilde{\varepsilon}}.
 \end{aligned} \tag{4.2}$$

For the sake of clarity, the index $\tilde{\varepsilon} = (\alpha, \beta, \delta) \in (0, 1)^3$ will be omitted in the following if there is no risk of confusion with the unknowns of the limit system (2.1). The semi-discretization of the governing equations (4.2) is done in a similar manner as in (4.1): First, the phase field variable $c^{\tilde{\varepsilon}}$ is evolved in time. The corresponding semi-discrete evolution equations read as

$$c^* + \Delta t \left[\nabla \cdot (c^* \mathbf{u}^n) + \nabla \cdot \mathbf{v}^* \right] = c^n, \tag{4.3a}$$

$$\mathbf{v}^* + \frac{\Delta t}{\delta + \Delta t} \left[W''(c^n) \nabla c^* + \frac{1}{\beta} \nabla (c^* - \omega^*) \right] = \frac{\delta}{\delta + \Delta t} \mathbf{v}^n, \tag{4.3b}$$

$$(\mathcal{I} - \gamma \beta \Delta) \omega^* = \mathcal{I}_\omega \omega^* = c^*, \tag{4.3c}$$

where \mathcal{I}_ω defines an operator given as $\mathcal{I}_\omega = \mathcal{I} - \gamma \beta \Delta$, \mathcal{I} being the identity operator. From (4.3) it is obvious that for the evolution of the phase field variable, a system of three equations has to be solved. In the numerical implementation,

we solve for c^* by substituting (4.3b) and (4.3c) into (4.3a). The resulting update formula for c^* is then given by

$$c^* + \Delta t \left[\nabla \cdot (c^* \mathbf{u}^n) - \frac{\Delta t}{\delta + \Delta t} \nabla \cdot \left[W''(c^n) \nabla c^* + \frac{1}{\beta} \nabla (c^* - \mathcal{I}_\omega^{-1} c^*) \right] \right] = c^n - \frac{\delta \Delta t}{\delta + \Delta t} \nabla \cdot \mathbf{v}^n. \quad (4.4)$$

While on the continuous level, the following equalities hold

$$\frac{1}{\beta} (c^* - \mathcal{I}_\omega^{-1} c^*) = \frac{1}{\beta} (c^* - \omega^*) = \frac{1}{\beta} (\mathcal{I}_\omega \omega^* - \omega^*) = -\gamma \Delta \omega^* = -\gamma \Delta \mathcal{I}_\omega^{-1} c^*, \quad (4.5)$$

our numerical experiments indicate that the discretized version of the very first term in (4.5) is prone to machine accuracy for $\beta \leq 10^{-7}$. This limits the overall convergence of the relaxation system (4.2) to the system (2.1) for $|\tilde{\varepsilon}| \rightarrow 0$. The reason for this is that the discrete version of \mathcal{I}_ω^{-1} is only accurate up to machine precision. Consequently, the discretized version of (4.5) reads as

$$\frac{1}{\beta} (c^* - \tilde{\mathcal{I}}_\omega^{-1} c^*) = -\gamma \left(\tilde{\Delta} + \frac{\mathcal{R}_M}{\beta} \right) \omega^* + \mathcal{R}_M, \quad (4.6)$$

where the superscript $\tilde{\cdot}$ indicates the discrete approximation of an operator and $\varepsilon_M := \mathcal{R}_M/\beta$ is an error term with $\mathcal{R}_M \sim \mathcal{O}(10^{-16})$ the error due to machine precision on a 64-bit architecture. Since \mathcal{R}_M is approximately a constant, with decreasing β , the error term ε_M will eventually dominate the overall error and prevents convergence. To overcome this shortcoming and enable a sound convergence of the relaxation formulation (4.2), instead of the very first term in (4.5), the very last one is used. Consequently, the final update formula for the phase field variable reads as

$$c^* + \Delta t \left[\nabla \cdot (c^* \mathbf{u}^n) - \frac{\Delta t}{\delta + \Delta t} \nabla \cdot \left[W''(c^n) \nabla c^* - \nabla \Delta \mathcal{I}_\omega^{-1} c^* \right] \right] = c^n - \frac{\delta \Delta t}{\delta + \Delta t} \nabla \cdot \mathbf{v}^n. \quad (4.7)$$

Therefore, this discretization resembles a fourth-order spatial operator similar to the discretized version of the original formulation of the NSCH system (4.2). However, given that the purpose of the present work is to investigate the convergence of solutions for system (4.2) to those of (2.1) in the limit of $|\tilde{\varepsilon}| \rightarrow 0$, which would not be possible with (4.4) for arbitrarily small values of β , this increased stencil size is accepted as a drawback of the chosen discretization. After the evolution of the phase field variable in time, the second step in the algorithm involves the update of the order parameter by solving (4.3c) for ω^* . In the third step, the velocities are evolved in time. For this, similar to the discretization of the original NSCH system, first a predictor step, given as

$$\mathbf{u}^* + \Delta t \nabla \cdot (\mathbf{u}^* \otimes \mathbf{u}^n) = \mathbf{u}^n - \Delta t c^* \left[W''(c^n) \nabla c^* - \gamma \nabla \Delta \omega^* \right], \quad (4.8)$$

is performed. Note that in (4.8), the additional term $\frac{1}{2}(\nabla \cdot \mathbf{u})\mathbf{u}$ has been omitted and will be accounted for in a later step. Second, following [31], the pressure is evolved in time by combining

$$\alpha p^{n+1} = \alpha p^n - \Delta t \nabla \cdot \mathbf{u}^{**}, \quad (4.9a)$$

$$\mathbf{u}^{**} = \mathbf{u}^* - \Delta t \nabla p^{n+1}. \quad (4.9b)$$

This yields the following diffusion equation with a source term for the pressure

$$\alpha p^{n+1} - \Delta t^2 \Delta p^{n+1} = \alpha p^n - \Delta t \nabla \cdot \mathbf{u}^*. \quad (4.10)$$

Finally, the velocities are updated to the next time level by first applying (4.9b) and then accounting for the missing term $\frac{1}{2}(\nabla \cdot \mathbf{u})\mathbf{u}$ by the use of

$$\mathbf{u}^{n+1} = \mathbf{u}^{**} - \Delta t \frac{1}{2} (\nabla \cdot \mathbf{u}^{**}) \mathbf{u}^{**}. \quad (4.11)$$

The final step involves the computation of the phase field variable at the next time step by

$$c^{n+1} + \Delta t \left[\nabla \cdot (c \mathbf{u})^{n+1} - \frac{\Delta t}{\delta + \Delta t} \nabla \cdot \left[W''(c^*) \nabla c^{n+1} - \nabla \Delta \mathcal{I}_\omega^{-1} c^{n+1} \right] \right] = c^n - \frac{\delta \Delta t}{\delta + \Delta t} \nabla \cdot \mathbf{v}^n, \quad (4.12)$$

which is then followed by an update of ω and \mathbf{v} obtained by the subsequent evaluation of

$$\omega^{n+1} = \mathcal{I}_\omega^{-1} c^{n+1}, \quad (4.13a)$$

$$\mathbf{v}^{n+1} = \frac{\delta}{\delta + \Delta t} \mathbf{v}^n - \frac{\Delta t}{\delta + \Delta t} \left[W''(c^*) \nabla c^{n+1} + \frac{1}{\beta} \nabla \Delta \omega^{n+1} \right]. \quad (4.13b)$$

Summarizing, the evolution of the numerical approximation of (4.2) involves the subsequent evaluation of (4.7), (4.8), (4.10), (4.11) and (4.13). A detailed discussion of the used stencils for the approximation of the spatial derivatives in (4.2) is given in Appendix B.

4.2. Numerical experiments in 1D

4.2.1. 1D Ostwald ripening

For the numerical investigation of the convergence behavior of (4.2) to (2.1) in the limit $|\tilde{\varepsilon}| \rightarrow 0$ in one spatial dimension, the Ostwald ripening of two bubbles with initial data

$$(c, u_1)^\top(0, x) = (A(x), 0)^\top, \quad (4.14)$$

where

$$A(x) = -1 + \sum_{i=1}^2 \tanh\left(\frac{|x - x_i| - r_i}{\sqrt{2\gamma}}\right) \quad (4.15)$$

and an end time of $t = 0.3$ was simulated. The setup for the Ostwald ripening is adopted from [13, 30], where the initial droplet's positions and radii are given as $x_1 = 0.3$, $x_2 = 0.75$ and $r_1 = 0.12$, $r_2 = 0.06$. For the initialization of the evolution variables of the relaxation system (2.7), we used $c^{\tilde{\varepsilon}}(0, x) = c(0, x)$, $\mathbf{u}^{\tilde{\varepsilon}}(0, x) = \mathbf{u}(0, x)$ and $p^{\tilde{\varepsilon}}(0, x) = 0$. The relaxation variable $\omega^{\tilde{\varepsilon}}$ is initialized by solving the corresponding elliptic constraint based on $c^{\tilde{\varepsilon}}(0, x)$, see e.g. (4.13a), and the flux variable $\mathbf{v}^{\tilde{\varepsilon}}$ was initialized as $\mathbf{v}^{\tilde{\varepsilon}} = -\nabla\mu$ by discretely approximating the gradient of the chemical potential with the spatial discretization introduced in Appendix A. A periodic computational domain $\Omega = (0, 1)$ and a capillary parameter $\gamma = 10^{-3}$ were chosen. The simulations were performed for different grid resolutions $N_x \in \{100, 500\}$ and permutations of the relaxation parameters $\alpha \in [10^{-3}, 10^{-12}]$, $\beta \in [10^{-1}, 10^{-9}]$ and $\delta \in [10^{-3}, 10^{-12}]$ resulting in a total amount of 1802 simulations. The time step size $\Delta t = 10^{-3}$ was constant.

The solution of the phase field variable at different time instances and the temporal evolution of the total Helmholtz energy over time are depicted in Fig. 2. Over time, the expected vanishing of the smaller bubble on the right and the

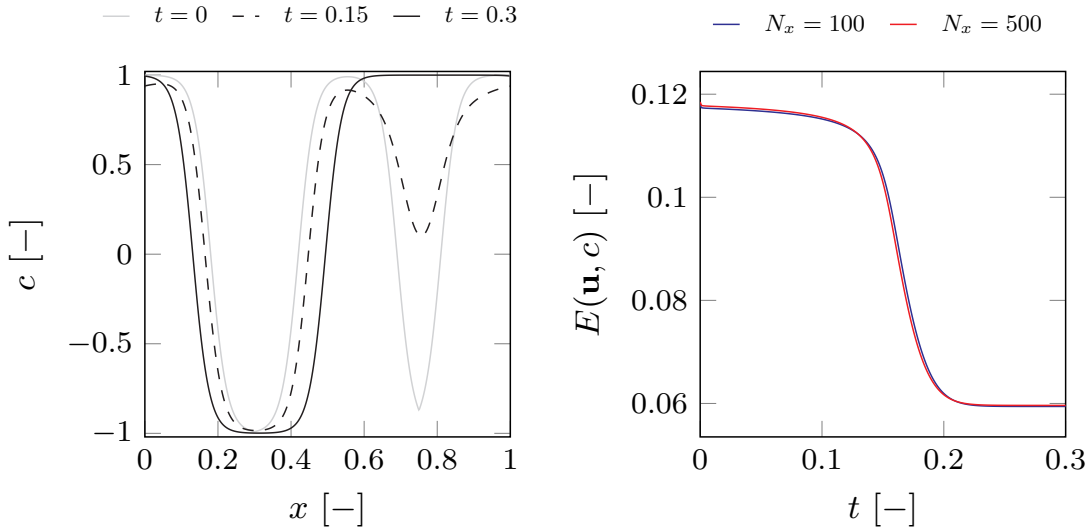


Figure 2: Left: Solution of the phase field variable at different time instances $t = 0$, $t = 0.15$, $t = 0.3$ with $N_x = 500$. Right: Temporal evolution of the total Helmholtz energy (2.5) for different grid resolutions.

corresponding growth of the bubble on the left can be observed. The thermodynamic admissibility of the results are indicated by a monotonic decreasing total Helmholtz energy over time. A further refinement of the spatial resolution did not affect the results. The error of the discretized equations (B.1) in comparison to the discretized equations (4.1) for different choices of the approximation parameters in $\tilde{\varepsilon}$ and the corresponding convergence behavior is depicted in Fig. 3. In the left and right columns, the error in the phase field variable and the velocity are plotted, respectively. In the top row, the convergence with respect to α for a fixed value of $\beta = 10^{-9}$ and decreasing values of $\delta \in [10^{-3}, 10^{-12}]$ is presented. The center row highlights the convergence with respect to β for a fixed value of $\alpha = 10^{-12}$ and decreasing values of $\delta \in [10^{-3}, 10^{-12}]$. In the bottom row, the convergence with respect to δ for a fixed value of $\alpha = 10^{-12}$ and decreasing values of $\beta \in [10^{-1}, 10^{-9}]$ is demonstrated. For all solution variables, the expected convergence of order $\mathcal{O}(\alpha + \beta + \delta)$ is achieved. Exemplarily for the top left plot: For sufficiently small values of β and δ , an error convergence of order $\mathcal{O}(\alpha)$ is observed, indicated by the red dashed line. However, if δ is not sufficiently small, the error stagnates even for decreasing values of α . The stagnant error convergence observed in the top left and bottom left

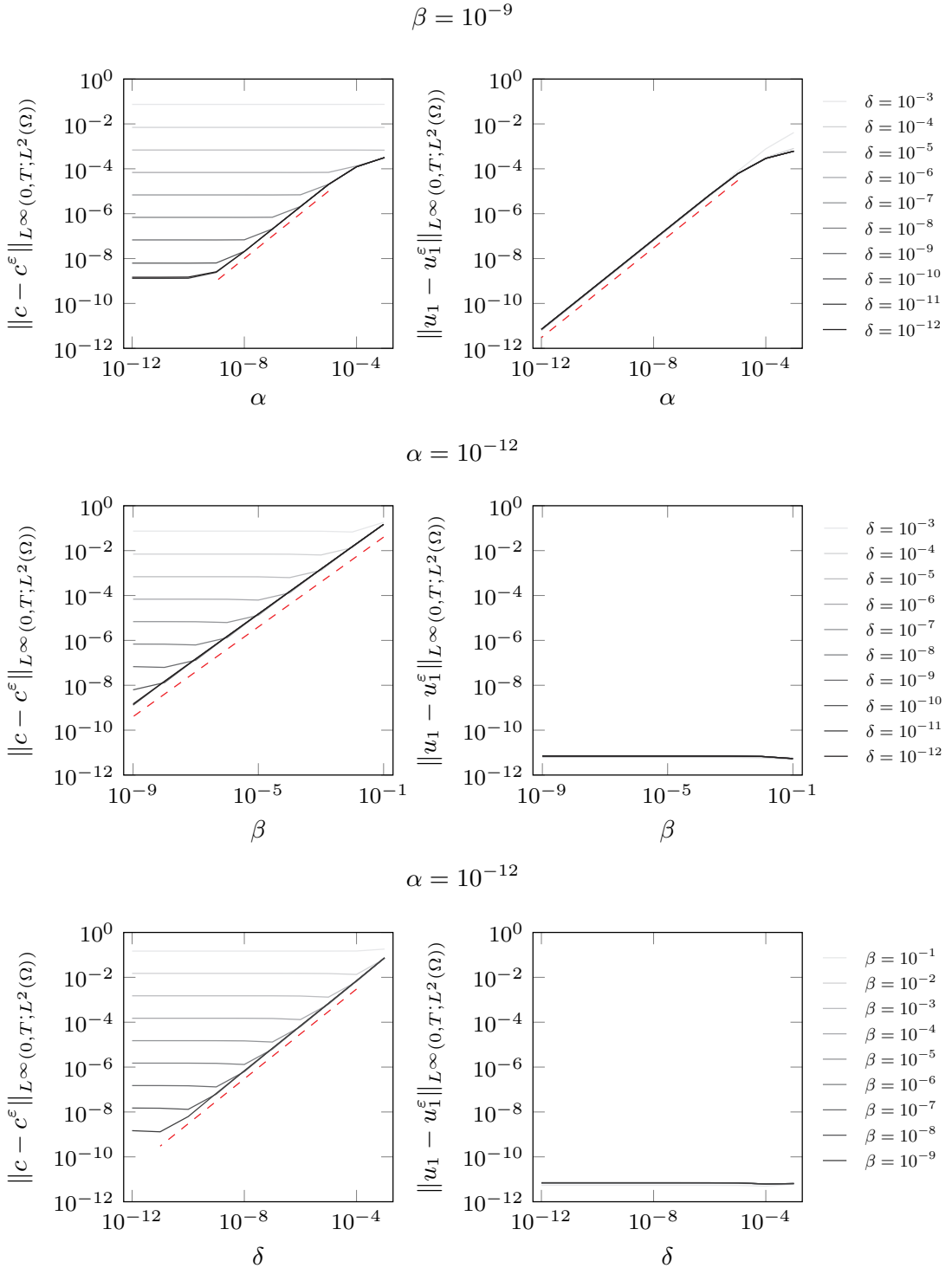


Figure 3: Convergence of the relaxation system (4.2) to the NSCH system (2.1) for the Ostwald ripening test case with $N_x = 100$. In the top row, the convergence in terms of α for a fixed value of β and varying δ is depicted. The center row shows the convergence in terms of β for a fixed α and varying δ . In the bottom row, the convergence error in terms of δ for a fixed value of α and varying β is plotted. The red dashed lines indicate convergence with order $\mathcal{O}(\alpha)$, $\mathcal{O}(\beta)$ and $\mathcal{O}(\delta)$, depending on the respective running variable on the abscissa.

plots, where the error does not decrease with α even with decreasing values of δ , can be attributed to a predominant error due to the relaxation parameter β . A further reduction of β would resolve this problem. Due to the one-dimensional setup, the error in the velocity is mainly governed by the choice of α , i.e., for sufficiently small values of α , the error in u_1 is unaffected by the choice of β and δ . Additional plots, investigating the convergence behavior also for the grid resolution $N_x = 500$, are given in Appendix C in Fig. 11. However, different grid resolutions as well as time step sizes only affect the absolute error, not the convergence behavior.

4.3. Numerical experiments in 2D

For the numerical investigation of the convergence behavior of (4.2) to (2.1) in the limit $|\tilde{\varepsilon}| \rightarrow 0$ in two spatial dimensions, the relaxation of a bubble to its equilibrium with the initial data

$$(c, u_1, u_2)^\top(0, \mathbf{x}) = (B(\mathbf{x}), 0, 0)^\top, \quad (4.16)$$

where

$$B(\mathbf{x}) = \begin{cases} -\cos(2\pi r) & : r = \sqrt{(x - 0.5)^2 + (y - 0.5)^2} \leq 0.5 \\ 1 & : \text{else} \end{cases} \quad (4.17)$$

and an end time of $t = 0.25$ and the merging of two droplets with initial data

$$(c, u_1, u_2)^\top(0, \mathbf{x}) = (C(\mathbf{x}), 0, 0)^\top, \quad (4.18)$$

where

$$C(\mathbf{x}) = -1 + \sum_{i=1}^2 \left(-\tanh\left(\frac{r - r_i}{\sqrt{2\gamma}}\right) + \tanh\left(\frac{r + r_i}{\sqrt{2\gamma}}\right) \right) \quad (4.19)$$

and an end time of $t = 0.25$ were simulated. In (4.19), the symbol $r = \sqrt{(x - x_i)^2 + (y - y_i)^2}$ indicates the Euclidean distance to the droplet's center with the droplets' centers and radii given as $\mathbf{x}_1 = (0.4, 0.5)^\top$, $\mathbf{x}_2 = (0.7, 0.5)^\top$ and $r_1 = 0.2$, $r_2 = 0.1$, respectively. In a final test case, a binary droplet collision with initial data

$$(c, u_1, u_2)^\top(0, \mathbf{x}) = (C(\mathbf{x}), D_1(\mathbf{x}), D_2(\mathbf{x}))^\top, \quad (4.20)$$

was investigated, where the droplets' centers and radii were defined as $\mathbf{x}_1 = (0.5, 0.7)^\top$, $\mathbf{x}_2 = (0.5, 0.3)^\top$ and $r_1 = r_2 = 0.15$, respectively. The divergence free velocity field was initialized as

$$D_1(\mathbf{x}) = \sin(2\pi x) \cos(2\pi y), \quad (4.21)$$

$$D_2(\mathbf{x}) = \cos(2\pi x) \sin(2\pi y) \quad (4.22)$$

and the simulation was performed until $t = 0.25$. The initialization of the evolution variables of the relaxation system (2.7) in 2D follows the same procedure as in the 1D case. For all three numerical experiments, a periodic computational domain $\Omega = (0, 1)^2$ and a capillary parameter $\gamma = 6 \cdot 10^{-3}$ was chosen, if not stated otherwise. The simulations were performed for two grid resolutions $N_x = N_y \in \{25, 50\}$ and permutations of the relaxation parameters $\alpha \in [10^{-3}, 10^{-12}]$, $\beta \in [10^{-1}, 10^{-9}]$ and $\delta \in [10^{-3}, 10^{-12}]$ resulting in a total amount of 5406 simulations. The time step size $\Delta t = 10^{-3}$ was constant.

The temporal evolution of the total Helmholtz energy according to the definition in (2.5) for all three test cases is depicted in Fig. 4. The thermodynamic admissibility of the results is indicated by the monotonically decreasing total Helmholtz energy for the investigated grid resolutions $N_x = N_y = 25$ and $N_x = N_y = 50$. In addition, the evolution of the total Helmholtz energy is shown for a grid resolution of $N_x = N_y = 100$ to demonstrate the grid convergence. However, due to the corresponding computational costs and the amount of simulations, this grid resolution is not used for the further analysis of the convergence in terms of $\tilde{\varepsilon}$.

4.3.1. Evolution of a 2D bubble

As a first test case, the relaxation of an initially perturbed bubble to its equilibrium was simulated. The solution of the phase field variable at $t = 0$, $t = 0.01$ and $t = 0.25$ computed with $N_x = N_y = 50$ is depicted in Fig. 5. For the visualization, a linear interpolation between the solution points of the phase field variable was used. The relaxation to a spherical bubble over time is evident. The error of the discretized equations (B.1) in comparison to the discretized equations (4.1) for different choices of the relaxation parameters in $\tilde{\varepsilon}$ and the corresponding convergence behavior is depicted in Fig. 6. In the left column, the error in the phase field variable is plotted, while in the center and right columns, the velocities in x and y are shown, respectively. Similar to the one-dimensional results: In the top row, the

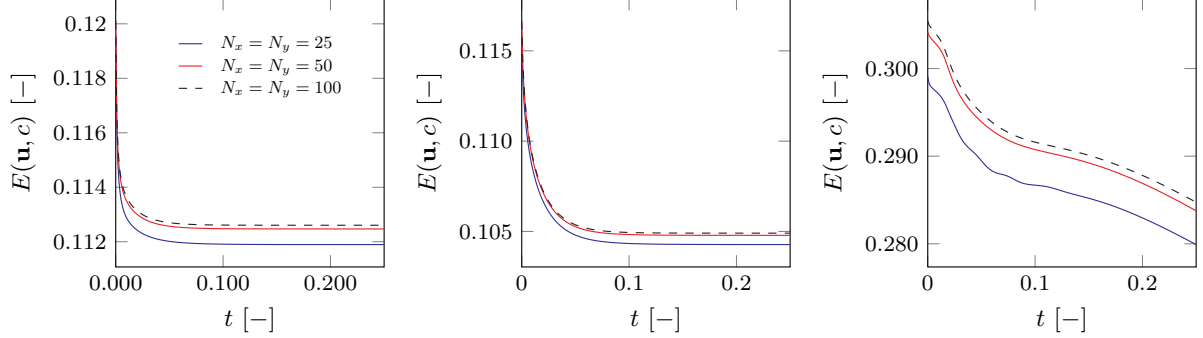


Figure 4: Temporal evolution of the total Helmholtz energy (2.5) of the NSCH system (2.1) for the single bubble, the merging droplets and the colliding droplets test cases, from left to right, each for three different grid resolutions.

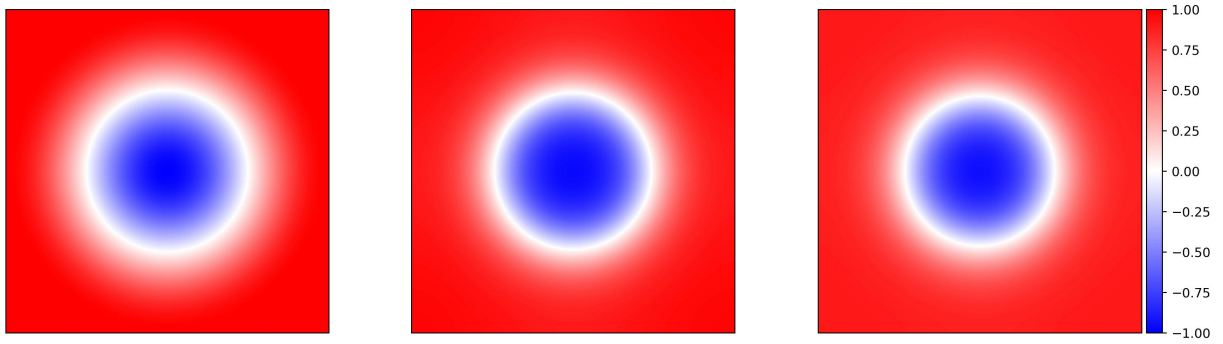


Figure 5: Solution of the phase field variable for the 2D bubble test case at $t = 0$ (left), $t = 0.01$ (center) and $t = 0.25$ (right) computed with $N_x = N_y = 50$.

convergence with respect to α for a fixed value of $\beta = 10^{-9}$ and decreasing values of $\delta \in [10^{-3}, 10^{-12}]$ is presented. The center row highlights the convergence with respect to β for a fixed value of $\alpha = 10^{-12}$ and decreasing values of $\delta \in [10^{-3}, 10^{-12}]$. In the bottom row, the convergence with respect to δ for a fixed value of $\alpha = 10^{-12}$ and decreasing values of $\beta \in [10^{-1}, 10^{-9}]$ is demonstrated. For all solution variables, the expected convergence of order $\mathcal{O}(\alpha + \beta + \delta)$ is achieved. Again, the red dashed lines indicate convergence in the order of the running variable on the abscissa for the remaining two relaxation parameters sufficiently small. The stagnant error convergence observed in the top left as well as all plots in the center and bottom row can be attributed to a predominant error caused by the relaxation parameters α and β . A further reduction of α and β would resolve this problem. Additional plots, investigating the convergence behavior also for the grid resolution $N_x = N_y = 50$, are given in Appendix D in Fig. 12. Similar to the one-dimensional experiments, the order of convergence remains unaffected by the grid resolution.

4.3.2. Merging droplets in 2D

As a second numerical experiment, a slightly more dynamic setup, the merging of two droplets initially in contact, was simulated. The solution of the phase field variable at $t = 0$, $t = 0.01$ and $t = 0.25$ computed with $N_x = N_y = 50$ is depicted in Fig. 5. For the visualization, a linear interpolation between the solution points of the phase field variable was used. Over time, the droplets merge and form a single spherical droplet at the end. The error of the discretized equations (B.1) in comparison to the discretized equations (4.1) for different choices of the relaxation parameters in $\tilde{\varepsilon}$ and the corresponding convergence behavior is depicted in Fig. 8. A similar arrangement of the plots to the previous section is used. Similar to the previous test cases, the anticipated convergence of order $\mathcal{O}(\alpha + \beta + \delta)$ is once more evident. In comparison to the single bubble test case, the overall error level is slightly elevated due to the higher velocities in this numerical experiment. Also in this setup, the parameters α and β dominate the error for small values of δ . Additional plots investigating the convergence behavior also for the grid resolution $N_x = N_y = 50$ are given in Appendix D in Fig. 13. Similar to the previous observations, the order of convergence remains unaffected.

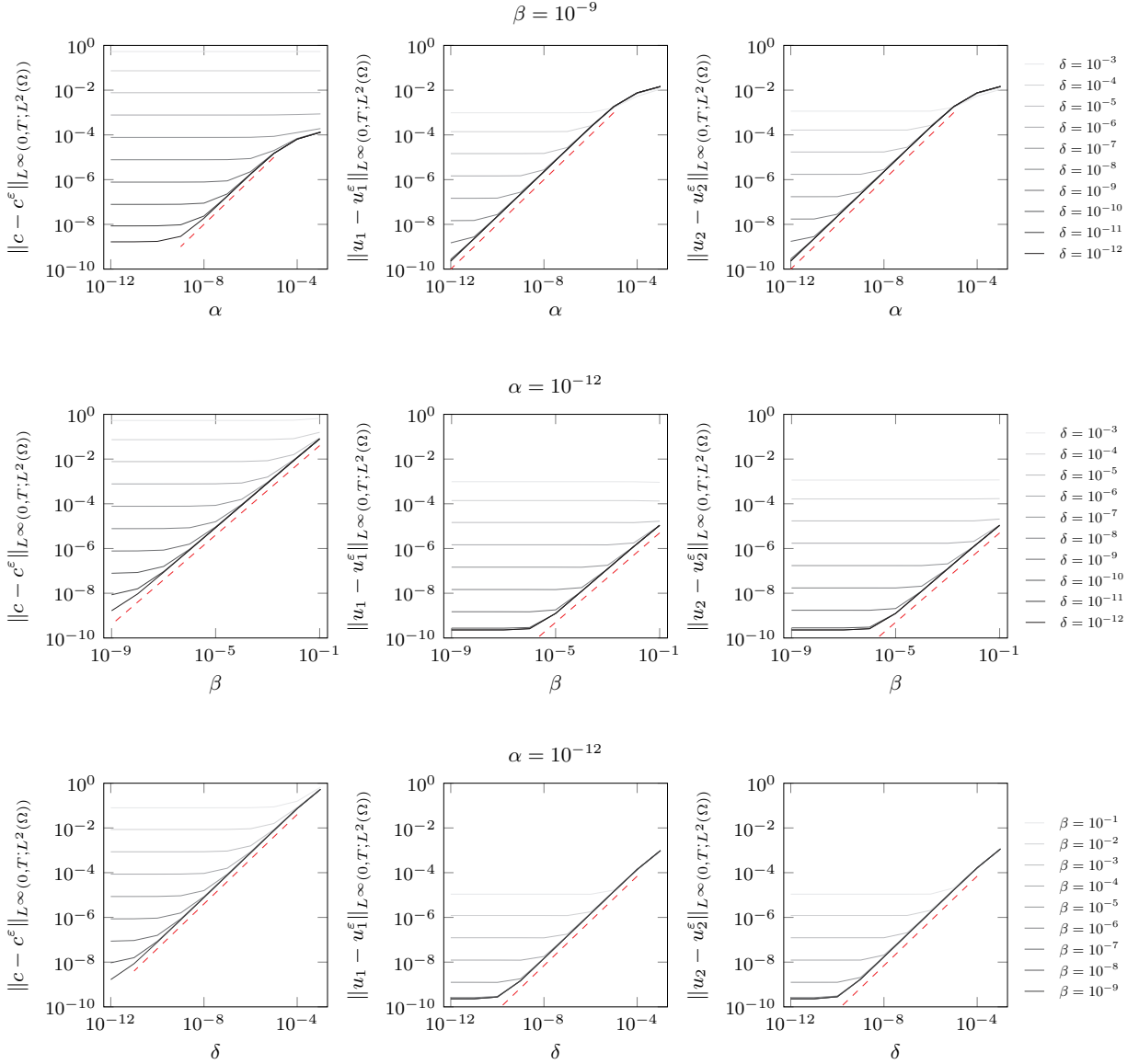


Figure 6: Convergence of the relaxation system (4.2) to the NSCH system (2.1) for the single bubble test case $N_x = N_y = 25$. In the top row, the convergence in terms of α for a fixed value of β and varying δ is depicted. The center row shows the convergence in terms of β for a fixed α and varying δ . In the bottom row, the convergence error in terms of δ for a fixed value of α and varying β is plotted. The red dashed lines indicate convergence with order $\mathcal{O}(\alpha)$, $\mathcal{O}(\beta)$ and $\mathcal{O}(\delta)$, depending on the respective running variable on the abscissa.

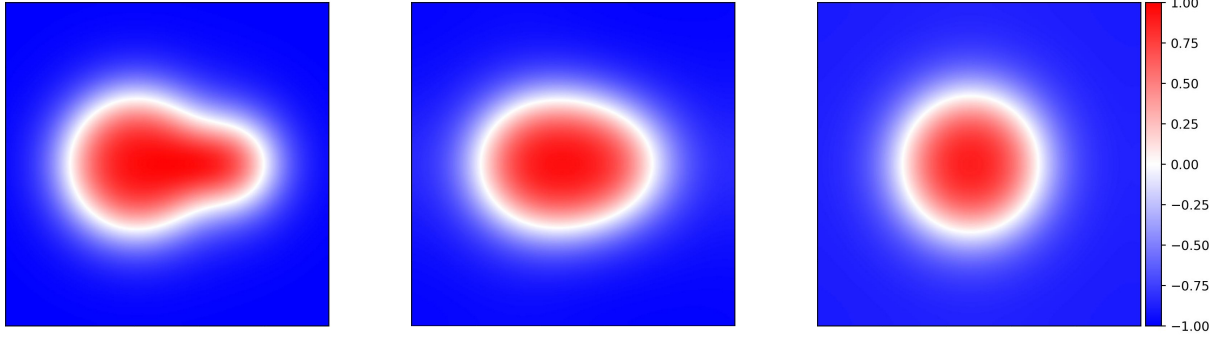


Figure 7: Solution of the phase field variable for the merging droplets test case at $t = 0$ (left), $t = 0.01$ (center) and $t = 0.25$ (right) computed with $N_x = N_y = 50$.

4.3.3. 2D droplet collision / droplet-wall interaction

In the final test case, a highly dynamic droplet collision is investigated. This setup is interesting for two reasons. First, it exhibits considerably higher velocities in comparison to the preceding test cases. Second, due to the symmetry of this numerical experiment, the test case is analogous to a droplet-wall interaction. At the symmetry plane, the constraints of a droplet-wall interaction with a slip wall and a 90° contact angle

$$\mathbf{u} \cdot \mathbf{n} = 0, \quad \nabla c \cdot \mathbf{n} = 0, \quad \nabla \mu \cdot \mathbf{n} = 0 \quad (4.23)$$

are satisfied. In contrast to the previous numerical experiments, a capillary parameter $\gamma = 10^{-3}$ was utilized to avoid an initial contact of the two droplets. The solution of the phase field variable at $t = 0$, $t = 0.03$ and $t = 0.25$ computed with $N_x = N_y = 50$ is depicted in Fig. 9. Similar to the previous test cases, a linear interpolation between the solution points of the phase field variable was used for the visualization. Over time, the droplets collide, merge and form the shape of an ellipsoid at $t = 0.25$. If the simulation would be performed further, the remaining droplet would oscillate and relax to a spherical shape.

The error of the discretized equations (B.1) in comparison to the discretized equations (4.1) for different choices of the relaxation parameters in $\tilde{\varepsilon}$ and the corresponding convergence behavior is displayed in Fig. 10. A similar arrangement of the plots to the previous section is used. Also for this slightly modified setup, the same convergence behavior as for the previous test cases is observed, where the error decreases with $\mathcal{O}(\alpha + \beta + \delta)$. Also in this setup, the parameters α and β dominate the error for small values of δ . Additional plots investigating the convergence behavior also for the grid resolution $N_x = N_y = 50$ are given in Appendix D in Fig. 14. Similar to the previous observations, the order of convergence remains unaffected.

5. Conclusions

We investigated a relaxation approximation for the classical NSCH system from [28] which provides a diffuse-interface approach for incompressible two-phase flow. Based on the relative-entropy approach and under appropriate smoothness assumptions, we have shown that the L^2 -difference between the approximate solution and the solution of the limit NSCH system vanishes linearly with respect to the relaxation parameters. Note that the relaxation system also provides approximations of ∇c converging (again in the L^2 -norm) with the same rate and of the pressure, the Laplacian of c and the Cahn-Hilliard flux converging with lower rates. For a series of interesting two-phase settings we confirmed the theoretical convergence results by numerical simulations. The numerical results have been obtained by a new MAC-type finite-difference method that is applicable in a seamless way for the limit NSCH system and the relaxation approximation.

As we have shown, our numerical method from the realm of solvers for hyperbolic balance laws allows high-velocity settings and is applicable even to inviscid flow. In this sense it can act as a numerical method to solve the limit NSCH system directly in such regimes. Then, for practical computations, one needs criteria to minimize the complete error in terms of the model error and the discretization error. This might be achieved by the development of appropriate a-posteriori error estimators [21]. Finally, for the NSCH model from [28] various improvements have been suggested in the last decade. It remains to investigate whether these models allow also for a hyperbolic relaxation approximation like our system (2.7) which is accessible to relative-entropy analysis and appropriate extensions of our numerical approach. Currently we work on specific extensions for problems with high-density contrasts and chemically reactive multi-component mixtures, see e.g. [2, 34, 36].

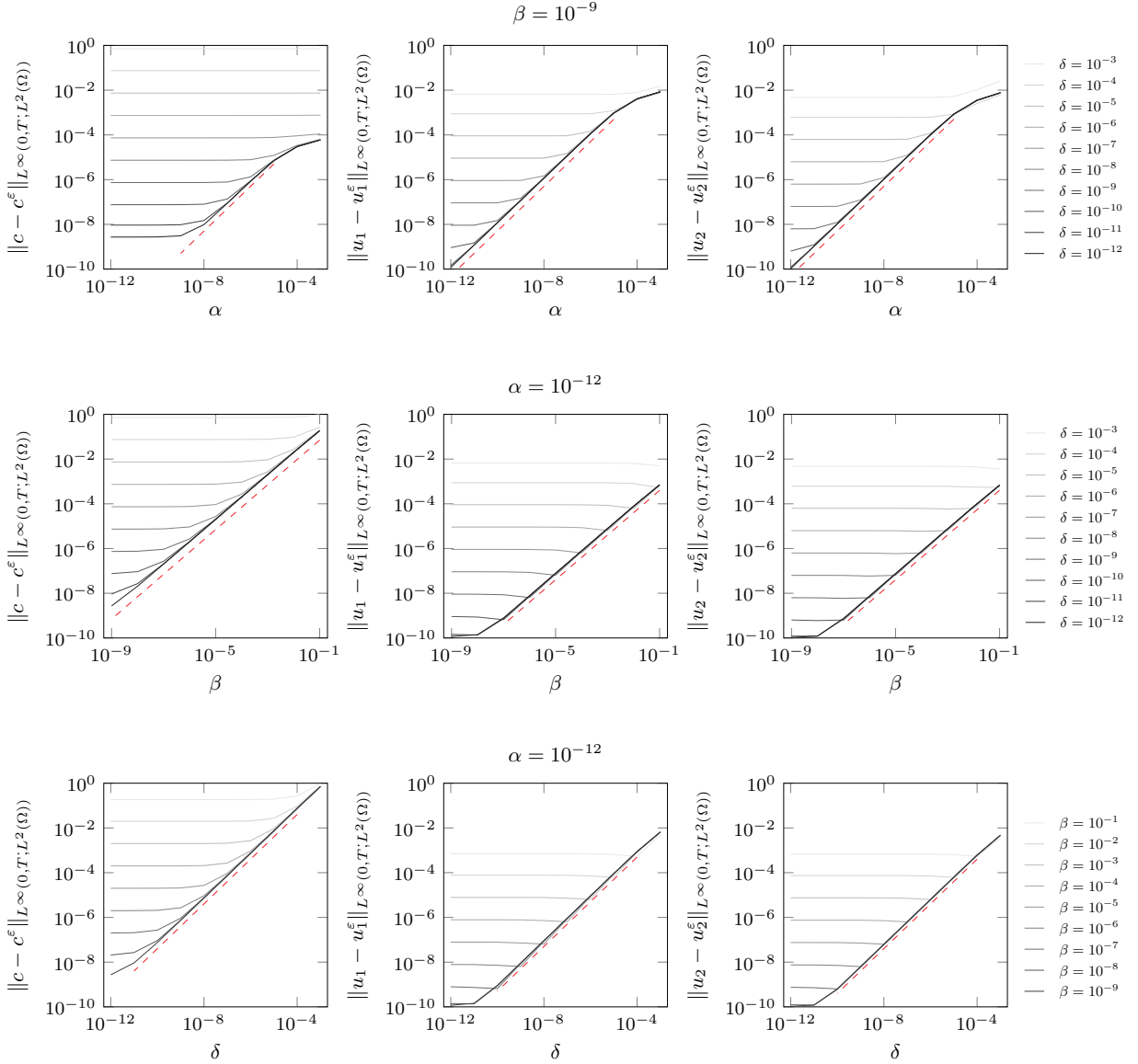


Figure 8: Convergence of the relaxation system (4.2) to the NSCH system (2.1) for the merging droplets test case with $N_x = N_y = 25$. In the top row, the convergence in terms of α for a fixed value of β and varying δ is depicted. The center row shows the convergence in terms of β for a fixed α and varying δ . In the bottom row, the convergence error in terms of δ for a fixed value of α and varying β is plotted. The red dashed lines indicate convergence with order $\mathcal{O}(\alpha)$, $\mathcal{O}(\beta)$ and $\mathcal{O}(\delta)$, depending on the respective running variable on the abscissa.

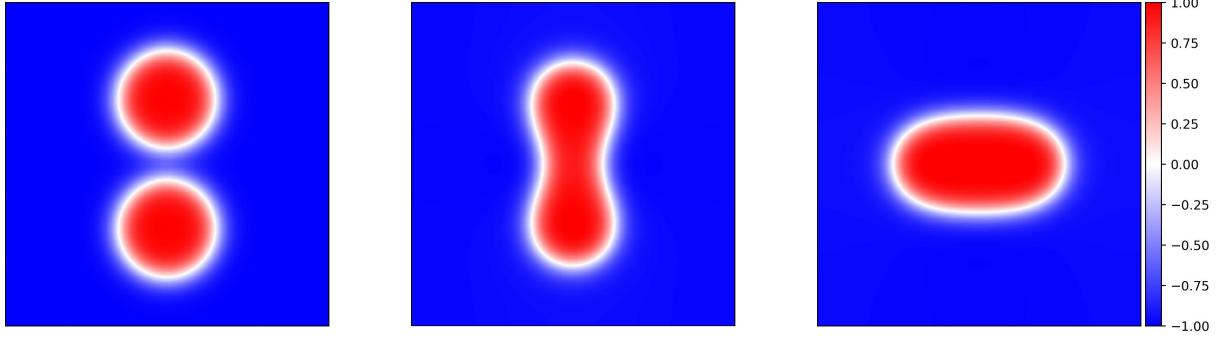


Figure 9: Solution of the phase field variable for the colliding droplets test case at $t = 0$ (left), $t = 0.03$ (center) and $t = 0.25$ (right) computed with $N_x = N_y = 50$.

Acknowledgements Financial support by the German Research Foundation (DFG), within the projects No. 525866748 and No. 526024901 of the Priority Programme - SPP 2410 Hyperbolic Balance Laws in Fluid Mechanics: Complexity, Scales, Randomness (CoScaRa) is acknowledged.

Appendix

In the following, the second-order accurate conservative finite difference scheme utilized for the approximation of the spatial derivatives in (4.1) and (4.2) is detailed. Although, this discretization is rather standard, for the sake of clarity and completeness, all employed stencils are defined. Herein, indices refer to the definitions in Fig. 1.

A. Spatial discretization of the NSCH system

A.1. Discretization of the evolution equations for the phase field variable (4.1a) and (4.1e)

The x contribution of the convective divergence operator in (4.1a) is approximated as

$$\left(\frac{\partial c u_1}{\partial x} \right)_{i,j} \approx \frac{(c u_1)_{i+\frac{1}{2},j} - (c u_1)_{i-\frac{1}{2},j}}{\Delta x} \quad \text{with} \quad (c u_1)_{i+\frac{1}{2},j} \approx \frac{1}{2} \left((c u_1)_{i+1,j} + (c u_1)_{i,j} \right) \quad (\text{A.1})$$

and

$$(u_1)_{i,j} \approx \frac{(u_1)_{i+\frac{1}{2},j} \Delta x \Delta y + (u_1)_{i-\frac{1}{2},j} \Delta x \Delta y}{2 \Delta x \Delta y} = \frac{1}{2} \left((u_1)_{i+\frac{1}{2},j} + (u_1)_{i-\frac{1}{2},j} \right). \quad (\text{A.2})$$

Equivalently, the contribution in the y -direction reads as

$$\left(\frac{\partial c u_2}{\partial y} \right)_{i,j} \approx \frac{(c u_2)_{i,j+\frac{1}{2}} - (c u_2)_{i,j-\frac{1}{2}}}{\Delta y} \quad \text{with} \quad (c u_2)_{i,j+\frac{1}{2}} \approx \frac{1}{2} \left((c u_2)_{i,j+1} + (c u_2)_{i,j} \right) \quad (\text{A.3})$$

and

$$(u_2)_{i,j} \approx \frac{(u_2)_{i,j+\frac{1}{2}} \Delta x \Delta y + (u_2)_{i,j-\frac{1}{2}} \Delta x \Delta y}{2 \Delta x \Delta y} = \frac{1}{2} \left((u_2)_{i,j+\frac{1}{2}} + (u_2)_{i,j-\frac{1}{2}} \right). \quad (\text{A.4})$$

In the following, the spatial discretization of the terms related to the Cahn-Hilliard part in (4.1a) are detailed, starting with the contribution of the double-well potential

$$\left(\nabla \cdot \left(W''(c) \nabla c \right) \right)_{i,j} = \left(\frac{\partial W''(c) \frac{\partial c}{\partial x}}{\partial x} \right)_{i,j} + \left(\frac{\partial W''(c) \frac{\partial c}{\partial y}}{\partial y} \right)_{i,j}. \quad (\text{A.5})$$

Here, the first term (x -direction) is approximated as

$$\left(\frac{\partial W''(c) \frac{\partial c}{\partial x}}{\partial x} \right)_{i,j} \approx \frac{\left(W''(c) \frac{\partial c}{\partial x} \right)_{i+\frac{1}{2},j} - \left(W''(c) \frac{\partial c}{\partial x} \right)_{i-\frac{1}{2},j}}{\Delta x} \quad (\text{A.6})$$

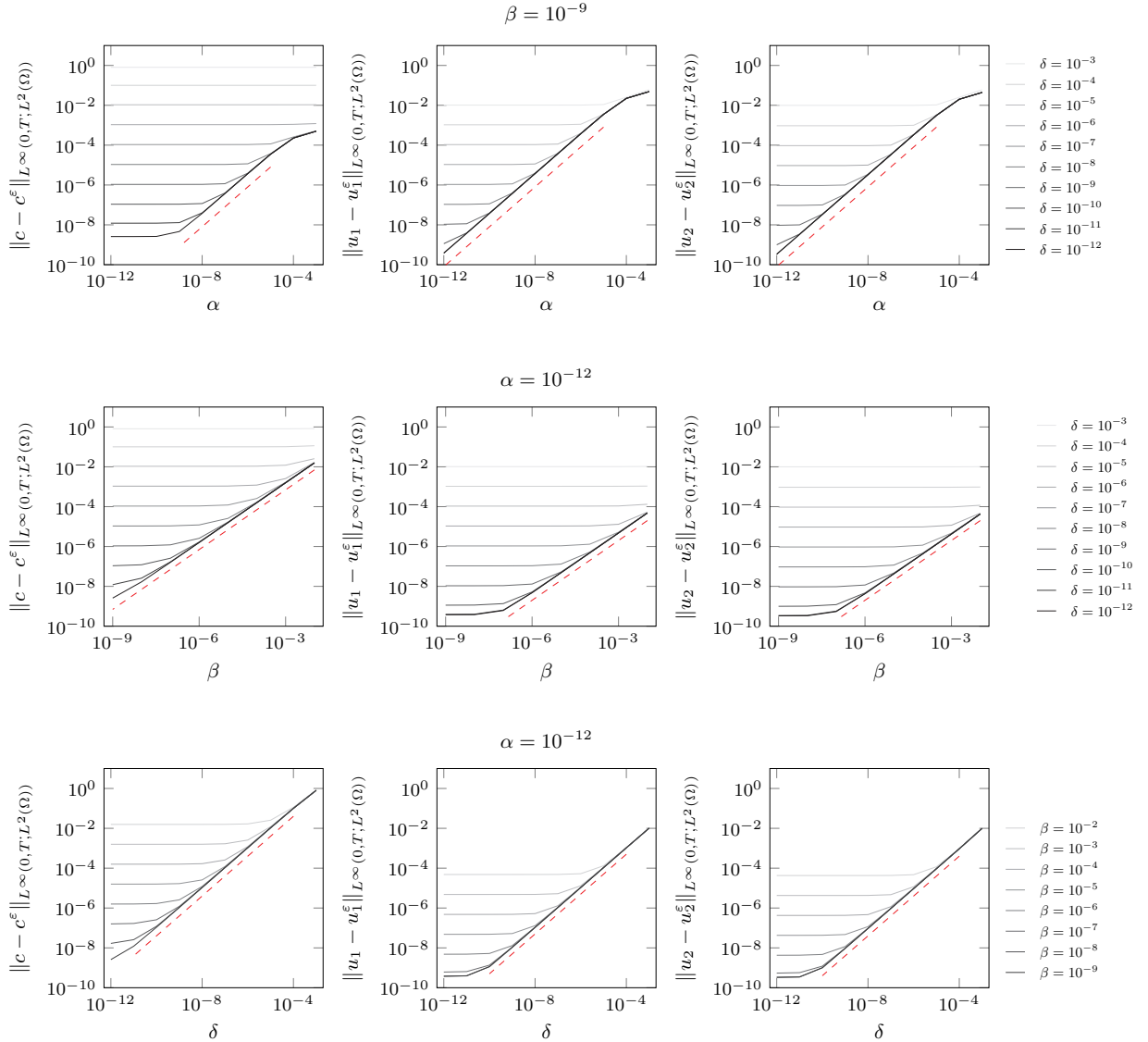


Figure 10: Convergence of the relaxation system (4.2) to the NSCH system (2.1) for the colliding droplets test case with $N_x = N_y = 25$. In the top row, the convergence in terms of α for a fixed value of β and varying δ is depicted. The center row shows the convergence in terms of β for a fixed α and varying δ . In the bottom row, the convergence error in terms of δ for a fixed value of α and varying β is plotted. The red dashed lines indicate convergence with order $\mathcal{O}(\alpha)$, $\mathcal{O}(\beta)$ and $\mathcal{O}(\delta)$, depending on the respective running variable on the abscissa.

with

$$\left(W''(c) \right)_{i+\frac{1}{2},j} \approx \frac{-W''(c_{i-1,j}) + 7W''(c_{i,j}) + 7W''(c_{i+1,j}) - W''(c_{i+2,j})}{12} \quad (\text{A.7})$$

and

$$\left(\frac{\partial c}{\partial x} \right)_{i+\frac{1}{2},j} \approx \frac{c_{i-1,j} - 7c_{i,j} + 7c_{i+1,j} - c_{i+2,j}}{12\Delta x}. \quad (\text{A.8})$$

Similarly, the second term (y -direction) reads as

$$\left(\frac{\partial W''(c) \frac{\partial c}{\partial y}}{\partial y} \right)_{i,j} \approx \frac{\left(W''(c) \frac{\partial c}{\partial x} \right)_{i,j+\frac{1}{2}} - \left(W''(c) \frac{\partial c}{\partial y} \right)_{i,j-\frac{1}{2}}}{\Delta y} \quad (\text{A.9})$$

with

$$\left(W''(c) \right)_{i,j+\frac{1}{2}} \approx \frac{-W''(c_{i,j-1}) + 7W''(c_{i,j}) + 7W''(c_{i,j+1}) - W''(c_{i,j+2})}{12} \quad (\text{A.10})$$

and

$$\left(\frac{\partial c}{\partial y} \right)_{i,j+\frac{1}{2}} \approx \frac{c_{i,j-1} - 7c_{i,j} + 7c_{i,j+1} - c_{i,j+2}}{12\Delta y}. \quad (\text{A.11})$$

The remaining fourth-order contribution

$$\left(\nabla \cdot (\gamma \nabla \Delta c) \right)_{i,j} = \frac{\partial}{\partial x} \left(\frac{\partial^3 c}{\partial x^3} + \frac{\partial^3 c}{\partial x \partial y^2} \right)_{i,j} + \frac{\partial}{\partial y} \left(\frac{\partial^3 c}{\partial x^2 \partial y} + \frac{\partial^3 c}{\partial y^3} \right)_{i,j} \quad (\text{A.12})$$

is approximated as

$$\begin{aligned} \left(\nabla \cdot (\gamma \nabla \Delta c) \right)_{i,j} \approx & \frac{\left(\frac{\partial^3 c}{\partial x^3} + \frac{\partial^3 c}{\partial x \partial y^2} \right)_{i+\frac{1}{2},j} - \left(\frac{\partial^3 c}{\partial x^3} + \frac{\partial^3 c}{\partial x \partial y^2} \right)_{i-\frac{1}{2},j}}{\Delta x} \\ & + \frac{\left(\frac{\partial^3 c}{\partial x^2 \partial y} + \frac{\partial^3 c}{\partial y^3} \right)_{i,j+\frac{1}{2}} - \left(\frac{\partial^3 c}{\partial x^2 \partial y} + \frac{\partial^3 c}{\partial y^3} \right)_{i,j-\frac{1}{2}}}{\Delta y} \end{aligned} \quad (\text{A.13})$$

with

$$\begin{aligned} \left(\frac{\partial^3 c}{\partial x^3} + \frac{\partial^3 c}{\partial x \partial y^2} \right)_{i+\frac{1}{2},j} \approx & \frac{-c_{i-1,j} + 3c_{i,j} - 3c_{i+1,j} + c_{i+2,j}}{\Delta x^3} \\ & + \frac{-c_{i,j-1} + c_{i+1,j-1} + 2c_{i,j} - 2c_{i+1,j} - c_{i,j+1} + c_{i+1,j+1}}{\Delta x^2 \Delta y} \end{aligned} \quad (\text{A.14})$$

and

$$\begin{aligned} \left(\frac{\partial^3 c}{\partial x^2 \partial y} + \frac{\partial^3 c}{\partial y^3} \right)_{i,j+\frac{1}{2}} \approx & \frac{-c_{i,j-1} + 3c_{i,j} - 3c_{i,j+1} + c_{i,j+2}}{\Delta y^3} \\ & + \frac{-c_{i-1,j} + c_{i-1,j+1} + 2c_{i,j} - 2c_{i,j+1} - c_{i+1,j} + c_{i+1,j+1}}{\Delta x \Delta y^2} \end{aligned} \quad (\text{A.15})$$

Straightforward computations show that combining (A.13) to (A.15) yields a second-order accurate central approximation of the biharmonic operator. This stencil choice for the Cahn-Hilliard part in (4.1a) has previously been used in [13] and forms an overall second-order accurate approximation.

A.2. Discretization of the momentum equations (4.1b)

The approximation of the convective term of the momentum equation in the x -direction

$$\left(\nabla \cdot (u_1 \mathbf{u}) \right)_{i+\frac{1}{2},j} = \frac{\partial}{\partial x} \left(u_1 u_1 \right)_{i+\frac{1}{2},j} + \frac{\partial}{\partial y} \left(u_1 u_2 \right)_{i+\frac{1}{2},j} \quad (\text{A.16})$$

reads as

$$(\nabla \cdot (u_1 \mathbf{u}))_{i+\frac{1}{2},j} \approx \frac{(u_1 u_1)_{i+1,j} - (u_1 u_1)_{i,j}}{\Delta x} + \frac{(u_1 u_2)_{i+\frac{1}{2},j+\frac{1}{2}} - (u_1 u_2)_{i+\frac{1}{2},j-\frac{1}{2}}}{\Delta y} \quad (\text{A.17})$$

with

$$(u_1 u_1)_{i,j} \approx \frac{1}{2} \left((u_1 u_1)_{i+\frac{1}{2},j} + (u_1 u_1)_{i-\frac{1}{2},j} \right) \quad (\text{A.18})$$

and

$$(u_1 u_2)_{i+\frac{1}{2},j+\frac{1}{2}} \approx \frac{1}{2} \left((u_1 u_2)_{i+\frac{1}{2},j+1} + (u_1 u_2)_{i+\frac{1}{2},j} \right), \quad (\text{A.19})$$

where

$$(u_2)_{i+\frac{1}{2},j} \approx \frac{(u_2)_{i,j-\frac{1}{2}} + (u_2)_{i+1,j-\frac{1}{2}} + (u_2)_{i,j+\frac{1}{2}} + (u_2)_{i+1,j+\frac{1}{2}}}{4}. \quad (\text{A.20})$$

Similarly to the x -direction, the approximation of the convective term of the momentum equation in the y -direction

$$(\nabla \cdot (u_2 \mathbf{u}))_{i,j+\frac{1}{2}} = \frac{\partial}{\partial x} (u_2 u_1)_{i,j+\frac{1}{2}} + \frac{\partial}{\partial y} (u_2 u_2)_{i,j+\frac{1}{2}} \quad (\text{A.21})$$

reads as

$$(\nabla \cdot (u_2 \mathbf{u}))_{i,j+\frac{1}{2}} \approx \frac{(u_2 u_1)_{i+\frac{1}{2},j+\frac{1}{2}} - (u_2 u_1)_{i-\frac{1}{2},j+\frac{1}{2}}}{\Delta x} + \frac{(u_2 u_2)_{i,j+1} - (u_2 u_2)_{i,j}}{\Delta y} \quad (\text{A.22})$$

with

$$(u_2 u_2)_{i,j} \approx \frac{1}{2} \left((u_2 u_2)_{i,j+\frac{1}{2}} + (u_1 u_1)_{i,j-\frac{1}{2}} \right) \quad (\text{A.23})$$

and

$$(u_2 u_1)_{i+\frac{1}{2},j+\frac{1}{2}} \approx \frac{1}{2} \left((u_1 u_2)_{i+1,j+\frac{1}{2}} + (u_1 u_2)_{i,j+\frac{1}{2}} \right), \quad (\text{A.24})$$

where

$$(u_1)_{i,j+\frac{1}{2}} \approx \frac{(u_1)_{i-\frac{1}{2},j} + (u_1)_{i+\frac{1}{2},j} + (u_1)_{i-\frac{1}{2},j+1} + (u_2)_{i+\frac{1}{2},j+1}}{4}. \quad (\text{A.25})$$

For the approximation of the Cahn-Hilliard contributions

$$\left(c \left[W''(c) \frac{\partial c}{\partial x} - \gamma \left(\frac{\partial^3 c}{\partial x^3} + \frac{\partial^3 c}{\partial x \partial y^2} \right) \right] \right)_{i+\frac{1}{2},j} \quad \text{and} \quad \left(c \left[W''(c) \frac{\partial c}{\partial y} - \gamma \left(\frac{\partial^3 c}{\partial x^2 \partial y} + \frac{\partial^3 c}{\partial y^3} \right) \right] \right)_{i,j+\frac{1}{2}} \quad (\text{A.26})$$

in the momentum equations in the x - and y -directions, respectively, except from $(c)_{i+\frac{1}{2},j}$ and $(c)_{i,j+\frac{1}{2}}$, all definitions were already introduced in (A.7), (A.8), (A.10), (A.11), (A.14) and (A.15). The missing two contributions for $(c)_{i+\frac{1}{2},j}$ and $(c)_{i,j+\frac{1}{2}}$ are approximated as

$$(c)_{i+\frac{1}{2},j} \approx \frac{-c_{i-1,j} + 7c_{i,j} + 7c_{i+1,j} - c_{i+2,j}}{12}, \quad (c)_{i,j+\frac{1}{2}} \approx \frac{-c_{i,j-1} + 7c_{i,j} + 7c_{i,j+1} - c_{i,j+2}}{12}. \quad (\text{A.27})$$

A.3. Discretization of the pressure equation (4.1c)

For the approximation of the Laplace and divergence operators in the pressure equation (4.1c), standard second-order central stencils are utilized, given as

$$(\Delta p)_{i,j} \approx \frac{p_{i-1,j} - 2p_{i,j} + p_{i+1,j}}{\Delta x^2} + \frac{p_{i,j-1} - 2p_{i,j} + p_{i,j+1}}{\Delta y^2} \quad (\text{A.28})$$

and

$$(\nabla \cdot \mathbf{u})_{i,j} \approx \frac{(u_1)_{i+\frac{1}{2},j} - (u_1)_{i-\frac{1}{2},j}}{\Delta x} + \frac{(u_2)_{i,j+\frac{1}{2}} - (u_2)_{i,j-\frac{1}{2}}}{\Delta y}. \quad (\text{A.29})$$

A.4. Discretization of the momentum equations (4.1d)

In the correction step of the momentum equations (4.1d), for the gradients of the pressure in the x - and y -direction, a standard central second-order stencil is applied, reading as

$$\left(\frac{\partial p}{\partial x} \right)_{i+\frac{1}{2},j} \approx \frac{p_{i+1,j} - p_{i,j}}{\Delta x} \quad \text{and} \quad \left(\frac{\partial p}{\partial y} \right)_{i+\frac{1}{2},j} \approx \frac{p_{i,j+1} - p_{i,j}}{\Delta y}, \quad (\text{A.30})$$

respectively.

B. Spatial discretization of the relaxation approximation of the NSCH system

In this appendix, the spatial discretization of the relaxation formulation of the NSCH equations (4.2) is detailed. For this, first, the utilized update formulas and their sequence is summarized in the following

$$c^* + \Delta t \left[\nabla \cdot (c^* \mathbf{u}^n) - \frac{\Delta t}{\delta + \Delta t} \nabla \cdot [W''(c^n) \nabla c^* - \nabla \Delta \mathcal{I}_\omega^{-1} c^*] \right] = c^n - \frac{\delta \Delta t}{\delta + \Delta t} \nabla \cdot \mathbf{v}^n, \quad (\text{B.1a})$$

$$\omega^* = \mathcal{I}_\omega^{-1} c^*, \quad (\text{B.1b})$$

$$\mathbf{u}^* + \Delta t \nabla \cdot (\mathbf{u}^* \otimes \mathbf{u}^n) = \mathbf{u}^n - \Delta t c^* [W''(c^n) \nabla c^* - \gamma \nabla \Delta \omega^*], \quad (\text{B.1c})$$

$$\alpha p^{n+1} - \Delta t^2 \Delta p^{n+1} = \alpha p^n - \Delta t \nabla \cdot \mathbf{u}^*, \quad (\text{B.1d})$$

$$\mathbf{u}^{**} = \mathbf{u}^* - \Delta t \nabla p^{n+1}, \quad (\text{B.1e})$$

$$\mathbf{u}^{n+1} = \mathbf{u}^{**} - \Delta t \frac{1}{2} (\nabla \cdot \mathbf{u}^{**}) \mathbf{u}^{**}, \quad (\text{B.1f})$$

$$c^{n+1} + \Delta t \left[\nabla \cdot (c \mathbf{u})^{n+1} - \frac{\Delta t}{\delta + \Delta t} \nabla \cdot [W''(c^*) \nabla c^{n+1} - \nabla \Delta \mathcal{I}_\omega^{-1} c^{n+1}] \right] = c^n - \frac{\delta \Delta t}{\delta + \Delta t} \nabla \cdot \mathbf{v}^n, \quad (\text{B.1g})$$

$$\omega^{n+1} = \mathcal{I}_\omega^{-1} c^{n+1}, \quad (\text{B.1h})$$

$$\mathbf{v}^{n+1} = \frac{\delta}{\delta + \Delta t} \mathbf{v}^n - \frac{\Delta t}{\delta + \Delta t} [W''(c^*) \nabla c^{n+1} + \frac{1}{\beta} \nabla \Delta \omega^{n+1}] \quad (\text{B.1i})$$

with

$$\mathcal{I}_\omega \omega = (\mathcal{I} - \gamma \beta \Delta) \omega = c. \quad (\text{B.2})$$

Starting with the discretization of the Laplace operator in (B.2), a standard second-order accurate central stencil, reading as

$$(\Delta \omega)_{i,j} = \frac{\omega_{i-1,j} - 2\omega_{i,j} + \omega_{i+1,j}}{\Delta x^2} + \frac{\omega_{i,j-1} - 2\omega_{i,j} + \omega_{i,j+1}}{\Delta y^2}, \quad (\text{B.3})$$

has been used. The corresponding inverse of the operator \mathcal{I}_ω utilized in (B.1a), (B.1b), (B.1g), (B.1h) and (B.1i) is computed by first performing an LU-factorization and second, applying the Jacobi-Gauss algorithm.

B.1. Discretization of the evolution equations for the phase field variable (B.1a) and (B.1g)

For the discretization of (B.1a) and (B.1g), the employed stencils have already been introduced in section A.1. The only missing contribution is the divergence operator $\nabla \cdot \mathbf{v}$ which, analogously to the velocity, is approximated by a central second-order accurate finite difference, given as

$$(\nabla \cdot \mathbf{v})_{i,j} = \frac{(v_1)_{i+\frac{1}{2},j} - (v_1)_{i-\frac{1}{2},j}}{\Delta x} + \frac{(v_2)_{i,j+\frac{1}{2}} - (v_2)_{i,j-\frac{1}{2}}}{\Delta y}. \quad (\text{B.4})$$

B.2. Discretization of the pressure and momentum equations (B.1c) to (B.1f)

Similar to the previous section, the majority of the used stencils has been introduced in sections A.2 to A.4. Herein, for the approximation of the third-order contribution $\nabla \Delta \omega$, an analogous stencil as in (A.14) and (A.15) is utilized only in terms of ω instead of c . The only missing contribution is the non-conservative product in (B.1f), where the stencils

$$((\nabla \cdot \mathbf{u}) u_1)_{i+\frac{1}{2},j} = \frac{(\nabla \cdot \mathbf{u})_{i+1,j} + (\nabla \cdot \mathbf{u})_{i,j}}{2} (u_1)_{i+\frac{1}{2},j}, \quad (\text{B.5})$$

$$((\nabla \cdot \mathbf{u}) u_2)_{i,j+\frac{1}{2}} = \frac{(\nabla \cdot \mathbf{u})_{i,j+1} + (\nabla \cdot \mathbf{u})_{i,j}}{2} (u_2)_{i,j+\frac{1}{2}} \quad (\text{B.6})$$

are employed.

B.3. Discretization of the evolution equation for the flux variable (B.1i)

All stencils utilized for the discretization of (B.1i) have previously been introduced in section A.1 and (B.3).

C. 1D Experiments

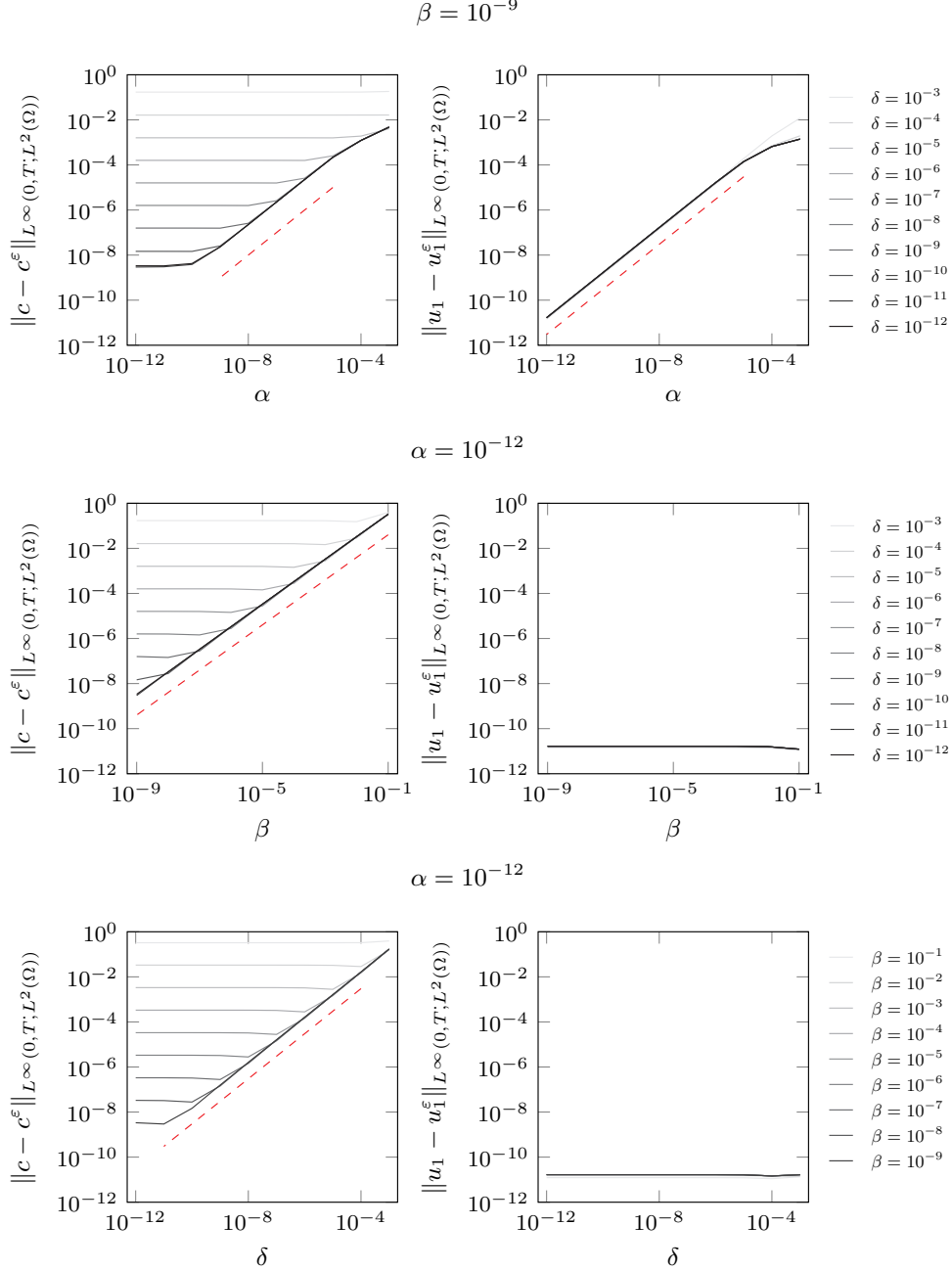


Figure 11: Convergence of the relaxation system (4.2) to the NSCH system (2.1) for the Ostwald ripening test case with $N_x = 500$. In the top row, the convergence in terms of α for a fixed value of β and varying δ is depicted. The center row shows the convergence in terms of β for a fixed α and varying δ . In the bottom row, the convergence error in terms of δ for a fixed value of α and varying β is plotted. The red dashed lines indicate convergence with order $\mathcal{O}(\alpha)$, $\mathcal{O}(\beta)$ and $\mathcal{O}(\delta)$, depending on the respective running variable on the abscissa.

D. 2D Experiments

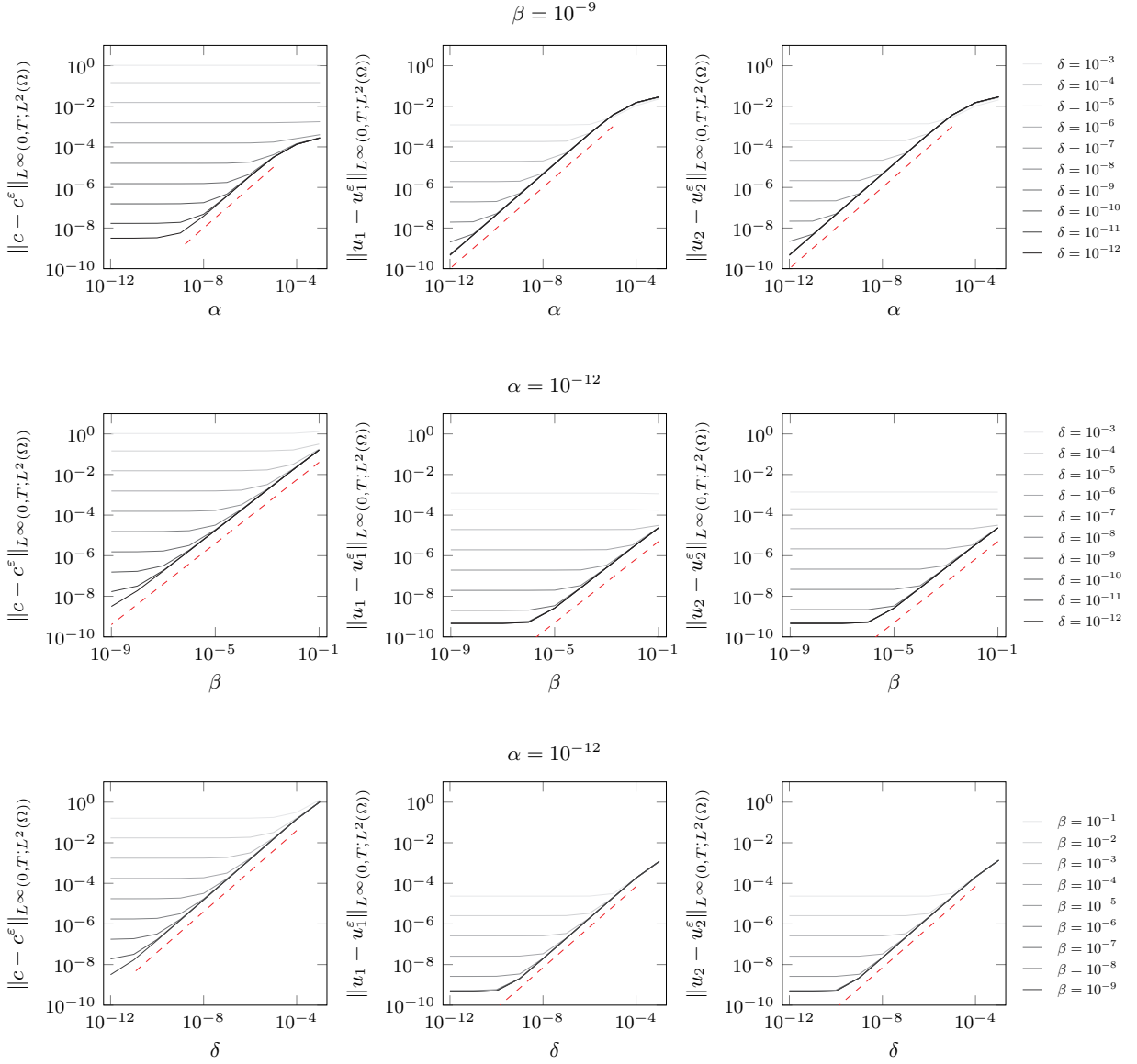


Figure 12: Convergence of the relaxation system (4.2) to the NSCH system (2.1) for the single bubble test case $N_x = N_y = 50$. In the top row, the convergence in terms of α for a fixed value of β and varying δ is depicted. The center row shows the convergence in terms of β for a fixed α and varying δ . In the bottom row, the convergence error in terms of δ for a fixed value of α and varying β is plotted. The red dashed lines indicate convergence with order $\mathcal{O}(\alpha)$, $\mathcal{O}(\beta)$ and $\mathcal{O}(\delta)$, depending on the respective running variable on the abscissa.

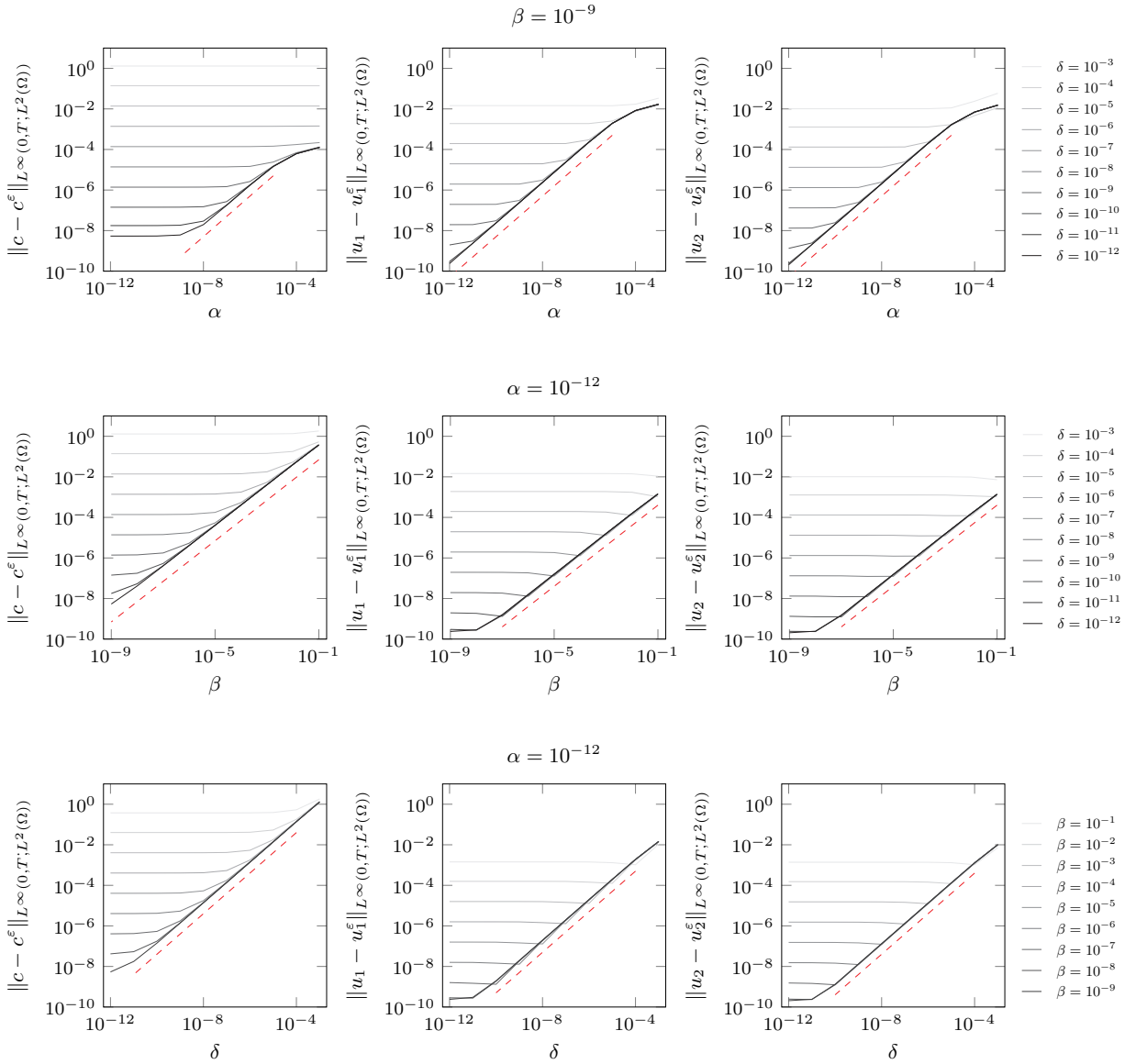


Figure 13: Convergence of the relaxation system (4.2) to the NSCH system (2.1) for the merging droplets test case with $N_x = N_y = 50$. In the top row, the convergence in terms of α for a fixed value of β and varying δ is depicted. The center row shows the convergence in terms of β for a fixed α and varying δ . In the bottom row, the convergence error in terms of δ for a fixed value of α and varying β is plotted. The red dashed lines indicate convergence with order $\mathcal{O}(\alpha)$, $\mathcal{O}(\beta)$ and $\mathcal{O}(\delta)$, depending on the respective running variable on the abscissa.

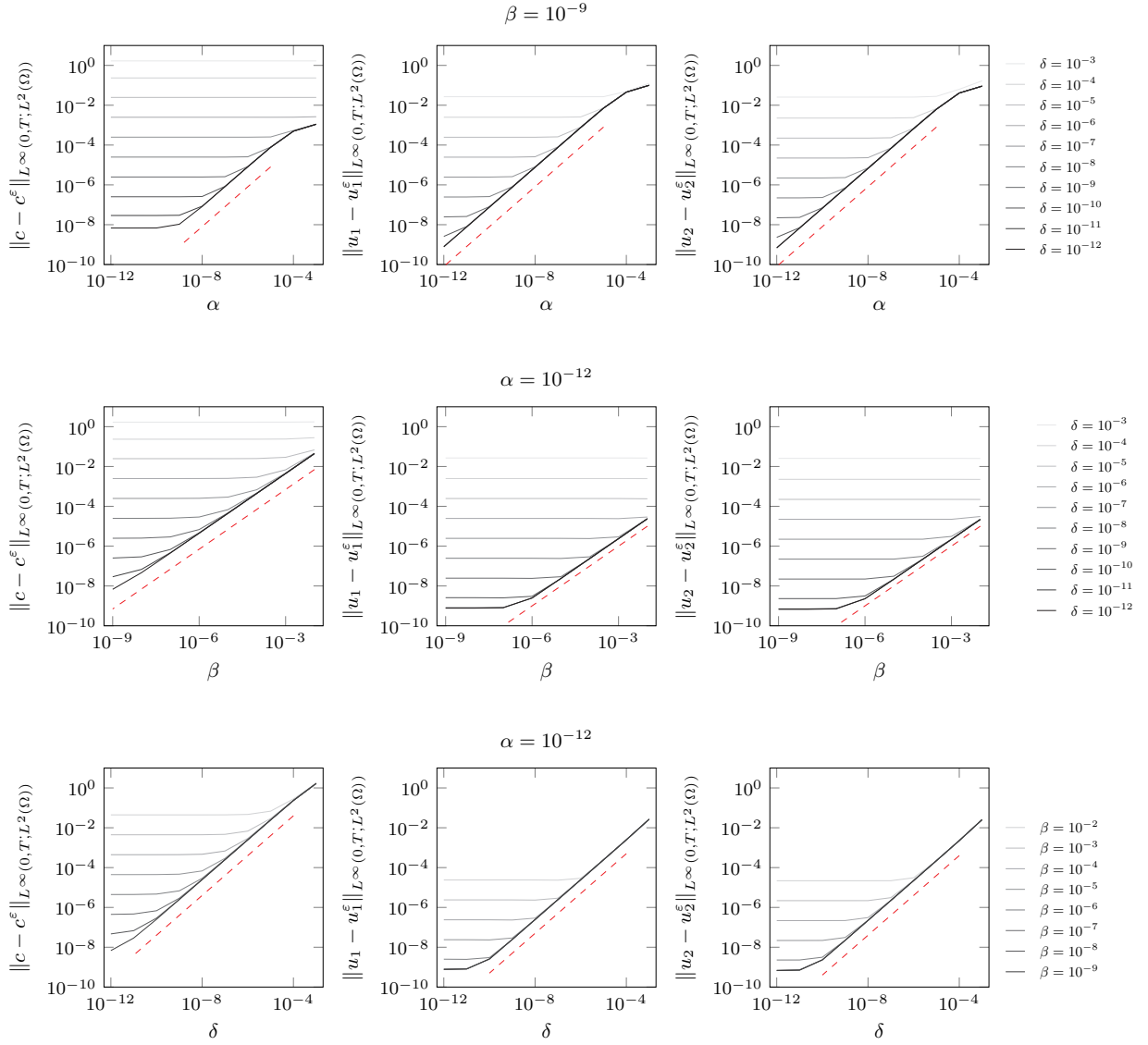


Figure 14: Convergence of the relaxation system (4.2) to the NSCH system (2.1) for the merging droplets test case with $N_x = N_y = 50$. In the top row, the convergence in terms of α for a fixed value of β and varying δ is depicted. The center row shows the convergence in terms of β for a fixed α and varying δ . In the bottom row, the convergence error in terms of δ for a fixed value of α and varying β is plotted. The red dashed lines indicate convergence with order $\mathcal{O}(\alpha)$, $\mathcal{O}(\beta)$ and $\mathcal{O}(\delta)$, depending on the respective running variable on the abscissa.

References

- [1] H. Abels. “On a diffuse interface model for two-phase flows of viscous, incompressible fluids with matched densities”. In: *Arch. Ration. Mech. Anal.* 194.2 (2009), pp. 463–506.
- [2] H. Abels, H. Garcke, and G. Grün. “Thermodynamically consistent, frame indifferent diffuse interface models for incompressible two-phase flows with different densities”. In: *Math. Models Methods Appl. Sci.* 22.3 (2012), pp. 1150013, 40.
- [3] H. Abels, Y. Liu, and S. Nečasová. “Low Mach number limit of a diffuse interface model for two-phase flows of compressible viscous fluids”. In: *GAMM-Mitt.* 47.4 (2024), Paper No. e202470008, 15.
- [4] R. Barthwal, F. Dhaouadi, and C. Rohde. *On hyperbolic approximations for a class of dispersive and diffusive-dispersive equations*. 2025. arXiv: 2512.04882.
- [5] F. Boyer. “Nonhomogeneous Cahn-Hilliard fluids”. In: *Ann. Inst. H. Poincaré C Anal. Non Linéaire* 18.2 (2001), pp. 225–259.
- [6] A. Brunk, H. Egger, O. Habrich, and M. Lukáčová-Medvidová. “A second-order fully-balanced structure-preserving variational discretization scheme for the Cahn–Hilliard–Navier–Stokes system”. In: *Math. Models Methods Appl. Sci.* 33.12 (2023), pp. 2587–2627.
- [7] N. Chaudhuri, C. Rohde, and F. Wendt. *Weak-Strong Uniqueness and Relaxation Limit for a Navier-Stokes-Korteweg Model*. 2025. arXiv: 2512.09719.
- [8] Y. Chen and J. Shen. “Efficient, adaptive energy stable schemes for the incompressible Cahn-Hilliard Navier-Stokes phase-field models”. In: *J. Comput. Phys.* 308 (2016), pp. 40–56.
- [9] A. J. Chorin. “A numerical method for solving incompressible viscous flow problems”. In: *J. Comput. Phys.* 2.1 (1967), pp. 12–26.
- [10] G. Cianfarani Carnevale and J. Giesselmann. “Extending relative entropy for Korteweg-type models with non-monotone pressure: large friction limit and weak-strong uniqueness”. In: *Commun. Math. Sci.* 23.7 (2025), pp. 1983–1998.
- [11] G. Cianfarani Carnevale and C. Lattanzio. “High friction limit for Euler-Korteweg and Navier-Stokes-Korteweg models via relative entropy approach”. In: *J. Differential Equations* 269.12 (2020), pp. 10495–10526.
- [12] C. M. Dafermos. *Hyperbolic conservation laws in continuum physics*. Fourth. Vol. 325. Grundlehren der mathematischen Wissenschaften [Fundamental Principles of Mathematical Sciences]. Springer-Verlag, Berlin, 2016, pp. xxxviii+826.
- [13] F. Dhaouadi, M. Dumbser, and S. Gavrilyuk. “A first-order hyperbolic reformulation of the Cahn-Hilliard equation”. In: *Proc. A.* 481.2312 (2025), Paper No. 20240606, 24.
- [14] A. E. Diegel, C. Wang, X. Wang, and S. M. Wise. “Convergence analysis and error estimates for a second order accurate finite element method for the Cahn–Hilliard–Navier–Stokes system”. In: *Numerische Mathematik* 137.3 (2017), pp. 495–534.
- [15] R. DiPerna. “Uniqueness of solutions to hyperbolic conservation-laws”. In: *Indiana Univ. Math. J.* 28.1 (1979), pp. 137–188.
- [16] M. F. P. ten Eikelder, K. G. van der Zee, I. Akkerman, and D. Schillinger. “A unified framework for Navier-Stokes Cahn-Hilliard models with non-matching densities”. In: *Math. Models Methods Appl. Sci.* 33.1 (2023), pp. 175–221.
- [17] X. Feng. “Fully discrete finite element approximations of the Navier-Stokes-Cahn-Hilliard diffuse interface model for two-phase fluid flows”. In: *SIAM J. Numer. Anal.* 44.3 (2006), pp. 1049–1072.
- [18] S. Gatti, M. Grasselli, V. Pata, and A. Miranville. “Hyperbolic relaxation of the viscous Cahn-Hilliard equation in 3-D”. In: *Math. Models Methods Appl. Sci.* 15.2 (2005), pp. 165–198.
- [19] J. Giesselmann. “A relative entropy approach to convergence of a low order approximation to a nonlinear elasticity model with viscosity and capillarity”. In: *SIAM J. Math. Anal.* 46.5 (2014), pp. 3518–3539.
- [20] J. Giesselmann, C. Lattanzio, and A. E. Tzavaras. “Relative energy for the Korteweg theory and related Hamiltonian flows in gas dynamics”. In: *Arch. Ration. Mech. Anal.* 223.3 (2017), pp. 1427–1484.
- [21] J. Giesselmann and T. Pryer. “A posteriori analysis for dynamic model adaptation in convection-dominated problems”. In: *Math. Models Methods Appl. Sci.* 27.13 (2017), pp. 2381–2423.
- [22] J. Giesselmann and H. Ranocha. *Convergence of hyperbolic approximations to higher-order PDEs for smooth solutions*. 2025. arXiv: 2508.04112.
- [23] A. Giorgini. “Existence and stability of strong solutions to the Abels-Garcke-Grün model in three dimensions”. In: *Interfaces Free Bound.* 24.4 (2022), pp. 565–608.
- [24] A. Giorgini, A. Miranville, and R. Temam. “Uniqueness and regularity for the Navier-Stokes-Cahn-Hilliard system”. In: *SIAM J. Math. Anal.* 51.3 (2019), pp. 2535–2574.

[25] A. Giorgini, R. Temam, and X.-T. Vu. “The Navier-Stokes-Cahn-Hilliard equations for mildly compressible binary fluid mixtures”. In: *Discrete Contin. Dyn. Syst. Ser. B* 26.1 (2021), pp. 337–366.

[26] F. Harlow and J. Welch. “Numerical calculation of time-dependent viscous incompressible flow of fluid with a free surface”. In: *Phys. Fluids* 8 (1965), pp. 2182–2189.

[27] T. Hitz, J. Keim, C.-D. Munz, and C. Rohde. “A parabolic relaxation model for the Navier-Stokes-Korteweg equations”. In: *J. Comput. Phys.* 421 (2020), pp. 109714, 24.

[28] P. C. Hohenberg and B. I. Halperin. “Theory of dynamic critical phenomena”. In: *Rev. Mod. Phys.* 49.3 (1977), p. 435.

[29] Q. Huang, C. Rohde, W.-A. Yong, and R. Zhang. “A hyperbolic relaxation approximation of the incompressible Navier-Stokes equations with artificial compressibility”. In: *J. Differential Equations* 438 (2025), Paper No. 113339, 26.

[30] J. Keim, H.-C. Konan, and C. Rohde. “A note on hyperbolic relaxation of the Navier-Stokes-Cahn-Hilliard system for incompressible two-phase flows”. In: *ESAIM: ProcS* 78 (2025), pp. 188–212.

[31] N. Kwatra, J. Su, J. T. Grétarsson, and R. Fedkiw. “A method for avoiding the acoustic time step restriction in compressible flow”. In: *J. Comput. Phys.* 228.11 (2009), pp. 4146–4161.

[32] X. Li and J. Shen. “On a SAV-MAC scheme for the Cahn–Hilliard–Navier–Stokes phase-field model and its error analysis for the corresponding Cahn–Hilliard–Stokes case”. In: *Math. Models Methods Appl. Sci.* 30.12 (2020), pp. 2263–2297.

[33] J. Lowengrub and L. Truskinovsky. “Quasi-incompressible Cahn–Hilliard fluids and topological transitions”. In: *Proc. R. Soc. A* 454.1978 (1998), pp. 2617–2654.

[34] C. Riethmüller, L. von Wolff, D. Göddeke, and C. Rohde. *Thermodynamically consistent phase-field modeling and numerical simulation for two-phase fluid-solid dynamics*. 2026. arXiv: 2601.09383.

[35] C. Rohde. “A local and low-order Navier-Stokes-Korteweg system”. In: *Nonlinear partial differential equations and hyperbolic wave phenomena*. Vol. 526. Contemp. Math. Providence, RI: Amer. Math. Soc., 2010, pp. 315–337.

[36] C. Rohde and L. von Wolff. “A ternary Cahn–Hilliard–Navier–Stokes model for two-phase flow with precipitation and dissolution”. In: *Math. Models Methods Appl. Sci.* 31.1 (2021), pp. 1–35.

[37] Y. Saad and M. H. Schultz. “GMRES: a generalized minimal residual algorithm for solving nonsymmetric linear systems”. In: *SIAM J. Sci. Statist. Comput.* 7.3 (1986), pp. 856–869.

[38] D. Serre. *Systems of conservation laws. 1*. Hyperbolicity, entropies, shock waves, Translated from the 1996 French original by I. N. Sneddon. Cambridge University Press, Cambridge, 1999, pp. xxii+263.

[39] C.-W. Shu. “Essentially non-oscillatory and weighted essentially non-oscillatory schemes for hyperbolic conservation laws”. In: *Advanced Numerical Approximation of Nonlinear Hyperbolic Equations: Lectures given at the 2nd Session of the Centro Internazionale Matematico Estivo (CIME) held in Cetraro, Italy, June 23–28, 1997*. Springer, 2006, pp. 325–432.

[40] R. Temam. “Sur l’approximation de la solution des équations de Navier-Stokes par la méthode des pas fractionnaires (I)”. In: *Arch. Ration. Mech. Anal.* 32 (1969), pp. 135–153.